PROCEEDINGS OF SCIENCE

On the controversial nature of the cataclysmic variable SS Cygni

Franco Giovannelli,[a,*] **María Dolores Sabau-Graziati,**[b] **Riccardo Ulisse Claudi,**[c,d] **Silvia Gaudenzi**[e] **and Corinne Rossi**[e]

[a] *INAF - Istituto di Astrofisica e Planetologia Spaziali, Via del Fosso del Cavaliere, 100, I 00133 Roma, Italy*
[b] *Departamento de Cargas Utiles y Ciencias del Espacio, C/ra de Ajalvir km 4, E 28850 Torrejón de Ardoz, Spain*
[c] *INAF - Osservatorio Astronomico di Padova, Vicolo dell'Osservatorio, 5, I 35122 Padova, Italy*
[d] *Dipartimento di Matematica e Fisica, Università Roma Tre, Via della Vasca Navale 84, I 00146 Roma, Italy*
[e] *Dipartimento di Fisica, Università Sapienza, Piazzale Aldo Moro 2, I 00185 Roma, Italy*
E-mail: franco.giovannelli@iaps.inaf.it, sabaumd@inta.es, riccardo.claudi@inaf.it, corinne.rossi@uniroma1.it, s.gaudenzi48@gmail.com

In this article we want to draw the reader's attention to a long-standing controversy regarding the nature of the cataclysmic variable SS Cygni. Much of the scientific world believes that SS Cygni is a non-magnetic cataclysmic variable, completely ignoring much experimental evidence that assigns SS Cygni to the category of intermediate polars. This controversy has been discussed by us in many past articles which will be cited in the bibliography. The aim we set ourselves is to demonstrate, above all to young people, the path that must be taken to try to reach scientific truth.

The Golden Age of Cataclysmic Variables and Related Objects - VI (GOLDEN2023)
4-9 September 2023
Palermo - (Mondello), Italy

∗Speaker

PoS(GOLDEN2023)028

1. Introduction

The old cataclysmic variable (CVs) classification was based on the optical outburst properties, by which one may distinguish four groups:

- Classical novae.
- Recurrent novae.
- Dwarf novae.
- Nova-like objects.

This classification, however, is neither self-consistent nor adequate and it is much better to consider primarily the observed accretion behaviour (Smak, 1985a).

Indeed, Lipunov (1987) and Lipunov & Postnov (1988) realized a general model for compact accreting stars: The Scenario Machine.

Starting from the trivial definition of X-Ray Binaries XRBs): they are binary systems emitting X-rays, a natural question arises. Are these systems governed by few physical parameters independent of their nature? The answer is positive. Indeed, high mass XRBs (HMXBs), low mass XRBs (LMXBs), anomalous X-ray pulsars (AXPs), and CVs can be considered as gravimagnetic rotators: a body with mass M, having a magnetic moment $\vec{\mu}$, rotating with rotational velocity $\vec{\omega}$, being the two axes not necessarily coincident, as sketched in Fig. 1. Introducing a physical parameter, $y = \dot{M}/\mu^2$, named *gravimagnetic parameter*, all the gravimagnetic rotators are contained in a plane Log P_{spin} vs Log y.

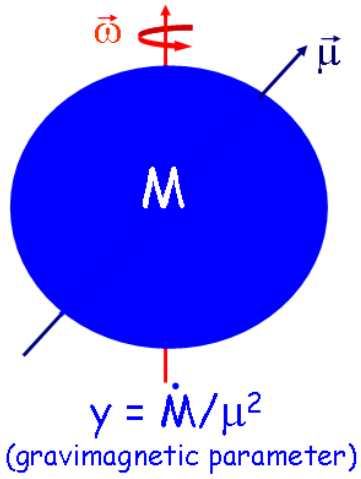

Figure 1: Gravimagnetic rotator: a body with mass M, having a magnetic moment $\vec{\mu}$, rotating with rotational velocity $\vec{\omega}$. The parameter $y = \dot{M}/\mu^2$ is called *gravimagnetic parameter* (Lipunov, 1987; Lipunov & Postnov, 1988).

The *Scenario Machine* (Monte Carlo simulations of binary evolution) permits to build up the complete picture of all possible evolutionary stages of binaries in the Galaxy. The basic evolution

equation (1) used for 500,000 systems containing magnetized stars provided the results contained in the plane Log P_{spin}–Log y, reported in the upper panel of Fig. 2. P_{spin} is expressed in seconds and the gravimagnetic parameter is expressed in unit of 10^{-42} g s^{-1} G^{-2} cm^{-6}. The symbols used for the different types of binaries are explained in the lower panel of Fig. 2. The definition of the characteristic radii can be found in the paper by Lipunov (1987).

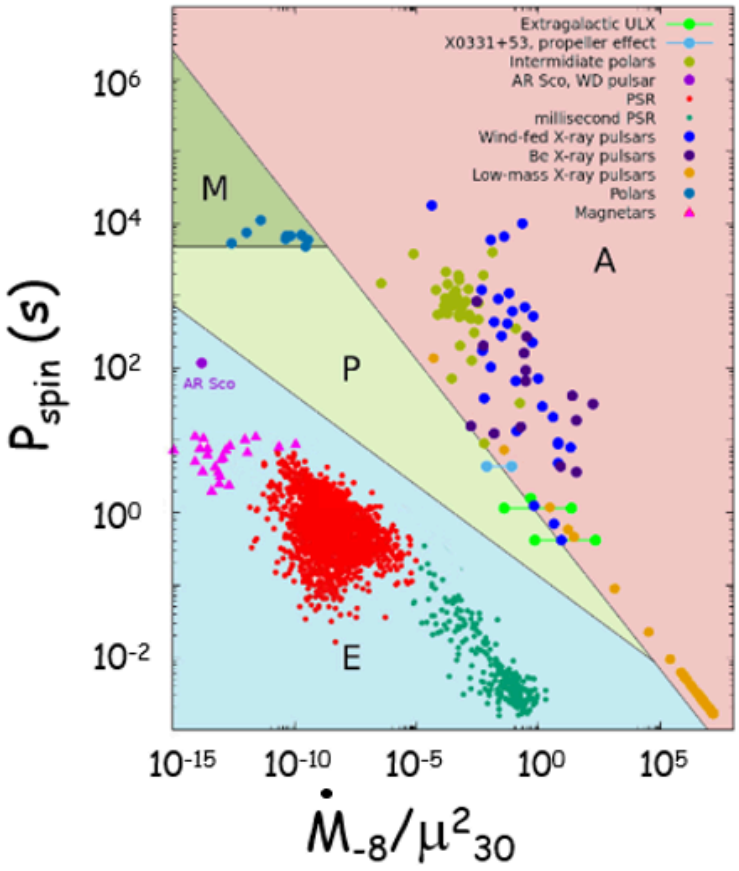

The rotator classification

Designation	Name	Physical sense
E	Ejector	$R_{st} > \max\{R_G, R_l\}$
P	Propeller	$R_c < R_{st} \le \max\{R_G, R_l\}$
A	Accretor	$R_{st} \le R_G$ and $R_{st} \le R_c$ $\quad \dot{M}_c \le \dot{M}_{cr}$
G	Georotator	$R_G < R_{st} \le R_c$
M	Magnetor	$R_{st} > a$ and $R_c > a$
SE	Superejector	$R_{st} > R_l$
SP	Superpropeller	$R_c < R_{st} \le R_l$ $\quad \dot{M}_c > \dot{M}_{cr}$
SA	Superaccretor	$R_{st} \le R_c$ and $R_{st} \le R_G$

Figure 2: Upper panel: distribution of magnetic rotators in the plane "Spin Period" – "Gavimagnetic Parameter" (adopted from Lipunov, Grinshpun & Vlasenko, 2021); lower panel: classification of rotators (Lipunov, 1987).

Type of rotator	Designation	The clearly confirmed observational example	Model assumptions
Ejector	E	Radiopulsars	LSI + 61°303, Cyg X-3, BL Lac objects,
Propeller	P	–	Transient X-ray sources, γ-bursts, some cataclysmic variables (dwarf novae), magnetic Ap-stars
Accretor	A	X-ray pulsars, X-ray bursters, cataclysmic variables with white dwarfs, novae, intermediate polars	–
Superejector	SE	–	SS 433, AGN, QSO
Superpropeller	SP	–	–
Superaccretor	SA	–	SS 433
Georotator	G	–	–
Magnetor	M	Polars	–

Figure 3: Observational examples of rotators (Lipunov, 1987).

$$\frac{\mathrm{dI}\omega}{\mathrm{dt}} = \dot{\mathrm{M}} K_{\mathrm{su}} - \frac{\kappa_{\mathrm{t}} \mu^2}{\mathrm{R}_{\mathrm{t}}^3} \tag{1}$$

where:

K_{su} = specific angular momentum applied by the accretion matter to the rotator;
$K_{su} = \sqrt{GM_x R_d}$ for Keplerian disk accretion;
$K_{su} = \eta_t \Omega R_g^2$ for wind accretion in a binary;
$K_{su} \sim 0$ for a single magnetic rotator;
R_d = radius of the inner disk edge;
Ω = rotational frequency of the binary system;
$\eta_t = 1/4$ (Illarionov & Sunyaev, 1975);
κ_t = dimensionless factor;
R_t = characteristic radius;
$\dot{M}$ = accretion rate in different regimes.

Observational examples of various types of rotators are reported in Fig. 3 (Lipunov, 1987).

Using the "Scenario Machine" Raguzova & Lipunov (1999) obtained an evolutionary track that can lead to the formation of Be/BH systems. The modern evolutionary scenario predicts the existence of binary black holes on eccentric orbits around Be stars and such systems may be discovered in the near future... Like happened!

Indeed, Raguzova & Lipunov (1999) calculations show that binary black holes with Be stars must have $0.2 < e < 0.8$. It is particularly difficult to detect such systems as most of their spectroscopic variations occur in a relatively small portion of the orbit, and could easily be missed if the systems are observed at widely separated epochs.

The CVs are usually classified into three classes depending on the magnetic field of the white dwarf: non-magnetic CVs (NMCVs), intermediate polar (IPs) and polar (Ps) with magnetic field intensities of $\lesssim 10^5$, $\approx 10^{5-6}$ and $\approx 10^{7-8}$ G, respectively. Figure 4 shows the three classes of CVs.

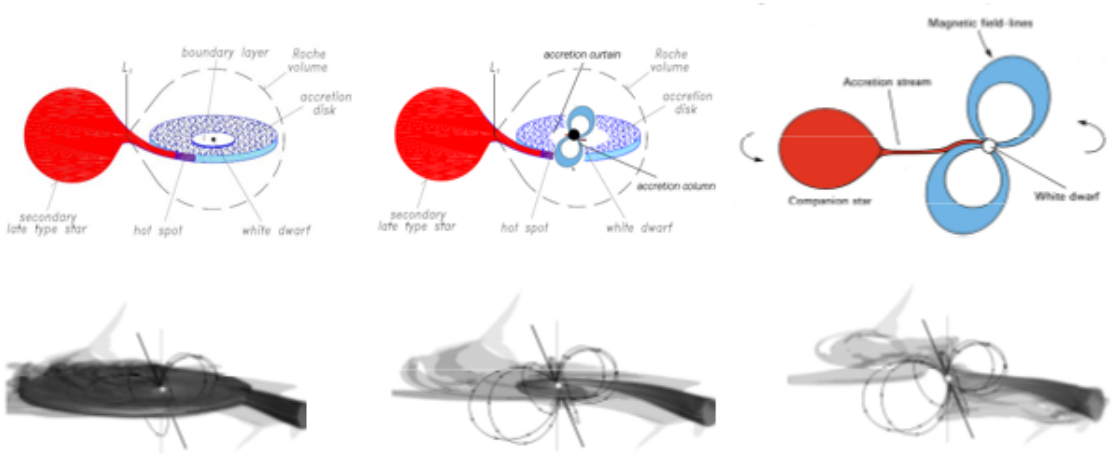

Figure 4: Upper panel: sketch of NMCVs, IPs and Ps (adopted from Giovannelli, 2017); lower panel: 3D MHD simulations of NMCVs, IPs and Ps (adapted from Bisikalo & Zhilkin, 2015).

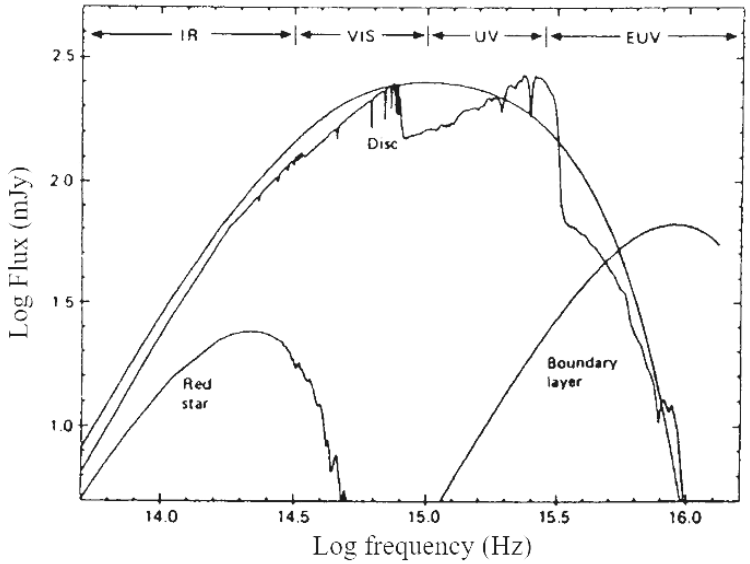

Figure 5: The flux emitted by a NMCV versus frequency (Pringle & Wade, 1985).

In the upper panel a sketch (Giovannelli, 2017), and in the lower panel the 3D MHD (Magneto Hydro-Dynamical) simulations (Bisikalo & Zhilkin, 2015).

Figure 5 shows the contribution of the various components (red star, accretion disc and boundary layer) of a NMCV from the infrared (IR) to extreme ultraviolet (EUV) frequencies (Pringle & Wade, 1985).

2. The cataclysmic variable SS Cyg

The history sometimes does not show fairness to its own facts: it indeed ignores some events while enhances some others. **SS Cyg is a significant example about it**.

SS Cyg is the first and the most luminous observed CV. Despite it is the most observed CV since the end of the 19th century (Parkhurst & Zaccheus, 1900; Zuckerman, 1961), there is still a controversy about its nature. An extensive review about SS Cyg was published by Giovannelli & Martinez-Pais (1991). The first accretion disk models were developed taking into account its dwarf nova nature. From the 1970's to nowadays new and new clues emerged about its possible magnetic nature. In spite of this, SS Cyg is still generally considered as non magnetic CV.

The coordinates of SS Cyg are: α_{2000} = 21^h 42^m $42^s.804$; δ_{2000} = +43° 35' 09".88. The visual magnitude in quiescence and in outburst is ≈ 12 and ≈ 8.5, respectively (e.g. Mattei, 1980; Cannizzo & Mattei, 1992). The visual absolute magnitude in quiescence is 5.9 (Giovannelli & Martinez-Pais, 1991). The orbital period is 0.27512973 days, corresponding to 6.60 h (Hessman et al., 1984). The distance, measured with the Hubble Space Telescope (HST), is D_H = 166 ±12 pc (Harrison et al., 1999), or using very long baseline interferometric radio observations the distance is D_M = 114 ±2 pc (Miller-Jones et al., 2013). From the second data release (DR2) of the ESA Gaia space mission, Pala et al. (2020) found a distance D_P = 114.6 ±0.6 pc.

SS Cyg has been monitored since 1896 by the American Association of Variable Star Observers (AAVSO). Figure 6 shows the light curves of SS Cyg from 27th September 1896 to 7th April 1992 (Cannizzo & Mattei, 1992). It is possible to see that the outbursts are of different kinds: large (L) and short (S) outbursts when the duration is > 12 or < 12 days, respectively. SS Cyg spends ∼ 75% of its time in the quiescent state.

Figure 7 shows the correlation between "normal" outburst duration and orbital period expressed in hour. Figure 8 shows the relation between the duration of "narrow" outbursts of dwarf novae and orbital period expressed in hour (Ak, Ozkan & Mattei, 2002). Similar relationship was reported many years before by Warner (1987).

Figure 8 shows the general picture of the absolute magnitudes of accretion discs at mean light. An approximate line of rate of mass transfer $\dot{M} \sim 5 \times l0^{-8}$ $M_\odot$ yr^{-1} is shown. The absolute magnitude M_V of the secondary is shown as a function of orbital period. A relationship between M_V and P_{orb} from the theory of magnetic braking is indicated for stars above the period gap. The arrow marked GR shows the visual luminosity expected for mass transfer powered by gravitational radiation (Warner, 1987). The asterisk represents SS Cyg. The location of SS Cyg is right where the intermediate polars are located.

3. The path to obtain the characteristic parameters and nature of SS Cyg

Probably, the "mistake" about the nature of SS Cyg born after the publication of a paper in Nature by Bath & van Paradijs (1983) where SS Cyg was classified as dwarf nova (DN) on the basis of optical behaviour, typical of DNe. This paper originated a bandwagon effect in the literature (see Michael Friedjung's comment in the first historical Frascati Workshop 1984: Giovannelli, 1985a) that "obliged" almost all the subsequent authors to start the papers saying that SS Cyg is a DN

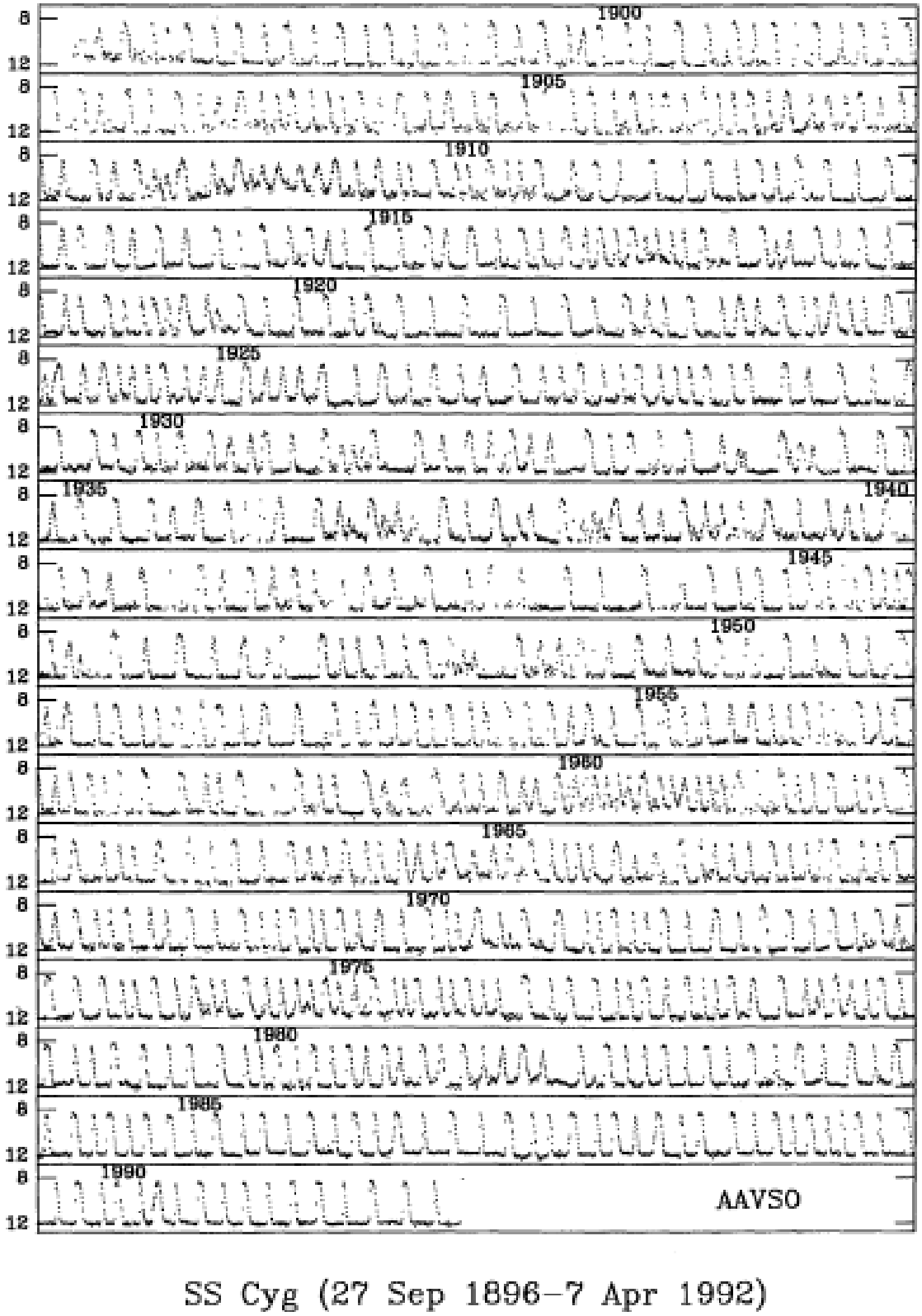

Figure 6: AAVSO SS Cyg Light curves from September 27, 1896 to April 7, 1992 (adopted from Cannizzo & Mattei, 1992).

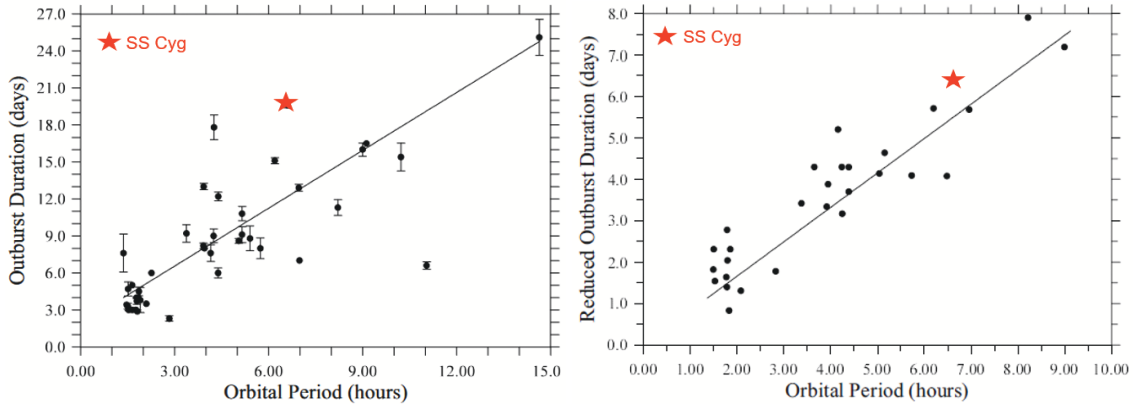

Figure 7: Left panel: Correlation between "normal" outburst duration and orbital period. Right panel: Correlation between "narrow" outburst duration and orbital period. The position of SS Cyg is marked with a red asterisk (Adapted from Ak, Ozkan & Mattei, 2002).

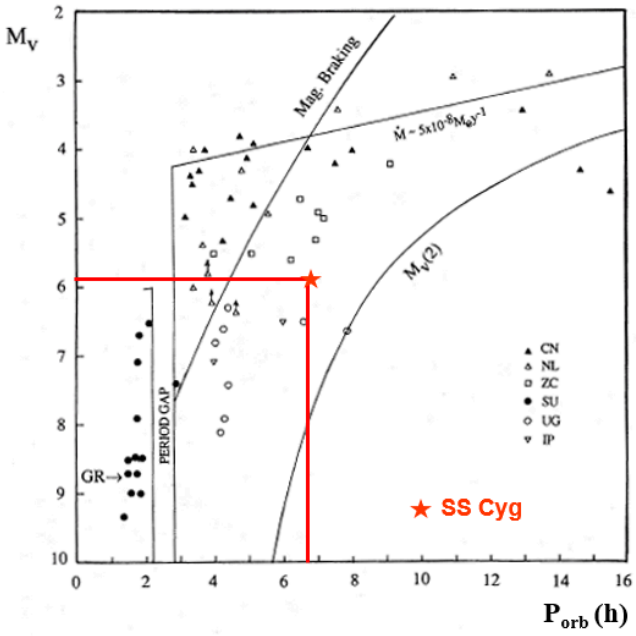

Figure 8: The absolute magnitudes of accretion discs at mean light in CVs vs orbital period (Adapted from Warner, 1987). CN = Classical Novae, NL = Nova-Like stars, ZC = Z Cam stars, SU = S Uma stars, UG = U Gem stars, IP = Intermediate Polars.

(NMCVs), without paying attention to other possibilities well documented in the so-called second class literature.

Therefore, our suggestion is to reconsider the problem about the nature of SS Cyg without any a priori bias.

Table 2. System parameters of SS Cyg, with columns 1–7 listing the authors, the systemic velocity, the inclination, the radial-velocity semi-amplitude of the secondary star, the primary mass, the secondary mass and the mass ratio.

Author	γ (km s^{-1})	i (degrees)	K_2	M_1 ($M_\odot$)	M_2 ($M_\odot$)	$q = \frac{M_2}{M_1}$
This work	−15.2	45	163.9	0.94	0.59	0.628
Hessman et al. (1984)	−15.1 ± 1	–	155 ± 2	–	–	0.595
North et al. (2002)	−13.09 ± 2.88	–	165 ± 1	–	–	0.68 ± 0.02
Bitner et al. (2007)	−13.1 ± 2.9	45–56	162.5 ± 1	0.81 ± 0.19	0.55 ± 0.13	0.685 ± 0.015
Martinez-Pais et al. (1994)	–	–	162.5 ± 3	–	–	–
Giovannelli et al. (1983)	–	40^{+1}_{-2}	–	$0.97^{+0.14}_{-0.05}$	$0.56^{+0.08}_{-0.03}$	$0.58^{+0.12}_{-0.10}$

Figure 9: System parameters of SS Cyg (adapted from Hill et al., 2017).

A recent paper by Hill et al. (2017) suggests to us to tell the history of the determination of the parameters of SS Cygni, and more, especially for the benefit of younger colleagues. Indeed, Fig. 9 shows the system parameters of SS Cyg, and in the last line, marked with a light red rectangle, the parameters derived by Giovannelli et al. (1983) are reported. These parameters, in spite of their origin from several measurements coming from different wavelength regions, are still valid if compared to "more accurate" experimental sources.

As discussed by Smak (1985b), emission lines are the most prominent features in the optical and ultraviolet spectra of CVs. Typically these are lines of H, neutral and ionized He, and ionized Ca. Their intensities are different in different systems. In the case of CVs with accretion disk around the white dwarf, the emission lines are often double peaked.

Indeed, the behaviour of the emission lines demonstrates that the transferred material does in fact produce a true disk rather than an amorphous cloud. Smak (1969) and Huang (1972) calculated the emission line profiles expected from gas disks of CVs and found that they should be double peaked and should have extensive wings.

The double component comes from the disk and originates from the surface of a flat, Keplerian disk (Smak, 1981), like shows in Fig. 10. Almost regardless of the radial distribution of the emitting atoms, the half-separation of the two peaks gives, to within ∼ 15% (Smak, 1969; Huang, 1972), the rotational velocity of the outer edge of the disk, V_d sin i (where i is the orbital inclination). For V_d we have:

$$V_d^2 = \frac{GM_{WD}}{R_d} \tag{2}$$

and for the observed velocity V_{obs}, we have:

$$\frac{1}{2}\frac{\Delta\lambda}{\lambda} = \frac{V_{obs}}{c} \tag{3}$$

$$V_{obs} = V_d \sin i \tag{4}$$

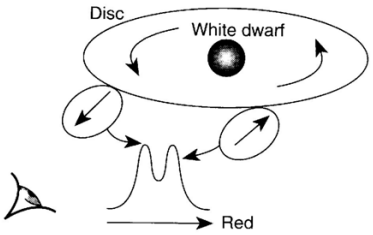

Figure 10: Sketch of the production of doubling in the emission lines from a flat, Keplerian accretion disk around the white dwarf in NMCVs (Smak, 1981, 1985b).

where:

R_d = outer radius of the disk; $\Delta\lambda$ = separation of the peaks; c = light velocity; V_{obs} = observed velocity; G = gravitational constant; M_{WD} = mass of the white dwarf; i = orbital inclination angle.

Giovannelli et al. (1983), with an hazardous operation for that time, started to collect all information coming from different wavelength regions for determining the parameters of SS Cyg, namely:

- their V_{obs} = 192 ± 10 km s^{-1} from the doubling observed in the Balmer emission lines in spectra taken during a quiescent phase of the system, as supported by the AAVSO measurements.
- The optical pulsations measured during different states of SS Cygni and ranging from 7.3 s (Hildebrand, Spillar & Stiening, 1981) to 10.9 s (Horne & Gomer, 1980; Patterson, 1979, 1981; Giovannelli, 1981).
- The X-ray pulsation of 9.735 ± 0.002 s measured by Patterson, Robinson & Kiplinger (1978)
- The available orbital data and the ratio between the external radius of the disk R_d and the separation, a, between the two components of the system, determined by Stover et al. (1980), Kiplinger (1979a,b), and Joy (1956).
- The mass-radius relationship for the white dwarf by Hartle & Thorne (1968).
- The mass-radius relationship for the secondary star by Plavec (1968).

By using Hartle & Thorne (1968) mass-radius relationship for the white dwarf and the minimum and maximum values of the optical pulsations, they limited the values of the orbital inclination angle between 38° and 41° (see Fig. 11, left panel). Then, if the X-ray pulsation of 9.7 s gives an upper limit to the Keplerian period at dwarf nova surface (Cordova et al., 1980), the lower limit of the mass of the white dwarf is 0.9 $M_\odot$. Thus, they constructed a table in which are reported all the parameters for different values of the orbital inclination angle (Fig. 11, right panel). Therefore, the orbital parameters of SS Cyg can be derived from the column marked with a light-red vertical rectangle.

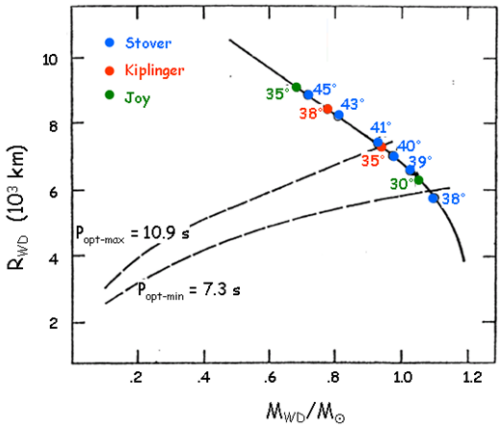

	i (deg)	50	45	44	43	42	41	40	39	38	35
$(a/10^{10})$ cm	S	12.0	13.0	13.2	13.5	13.7	14.0	14.3	14.6	14.9	16.0
	K	9.9	10.7	10.9	11.1	11.4	11.6	11.8	12.1	12.3	13.3
	J	11.8	12.7	13.0	13.2	13.5	13.7	14.0	14.3	14.6	15.7
$M_R/M_\odot$	S	0.33	0.42	0.45	0.47	0.50	0.53	0.56	0.60	0.64	0.79
	K	0.22	0.27	0.29	0.31	0.32	0.34	0.36	0.39	0.42	0.52
	J	0.44	0.57	0.60	0.63	0.67	0.71	0.75	0.80	0.86	1.06
$M_{wd}/M_\odot$	S	0.57	0.73	0.78	0.81	0.86	0.93	0.97	1.04	1.11	1.37
	K	0.29	0.37	0.39	0.42	0.43	0.46	0.49	0.52	0.56	0.69
	J	0.40	0.51	0.54	0.57	0.60	0.64	0.68	0.72	0.77	0.95
$R_R/R_\odot$	S	0.57	0.62	0.63	0.64	0.66	0.67	0.68	0.70	0.71	0.77
	K	0.50	0.54	0.56	0.57	0.58	0.59	0.60	0.62	0.63	0.67
	J	0.66	0.71	0.72	0.74	0.75	0.77	0.78	0.80	0.82	0.88
$R_d/R_\odot$	S	2.40	2.60	2.65	2.70	2.75	2.80	2.86	2.92	2.99	3.20
	K	2.58	2.78	2.84	2.89	2.96	3.02	3.07	3.14	3.21	3.43
	J	11.20	12.10	12.30	12.50	12.80	13.00	13.30	13.60	13.90	14.90

Figure 11: Left panel: mass-radius relationship for the WD and possible orbital inclination angles delimited by the values of optical pulsations (Adapted from Giovannelli et al., 1983). Right panel: table with orbital parameters for different values of orbital inclination angles. Light-red horizontal rectangles show the most probable values, coming from Stover et al. (1980), and the light-red vertical rectangle shows the orbital parameters of SS Cyg (adapted from Giovannelli et al., 1983).

Thus, the orbital parameters of SS Cyg are:

$i = 40^{\circ}{}^{+1^{\circ}}_{-2^{\circ}}$; $a = 14.3^{+0.6}_{-0.3} \times 10^{10}$ cm; $M_R = 0.56^{+0.08}_{-0.03}$ $M_\odot$; $M_{WD} = 0.97^{+0.14}_{-0.05}$ $M_\odot$; $R_R = 0.68^{+0.03}_{-0.01}$ $R_\odot$; $R_d = 2.86^{+0.13}_{-0.06} \times 10^{10}$ cm.

From the H_β in emission, Giovannelli et al. (1983) determined the width at the level of continuum as ≈ 2500 km s^{-1}. This imply a value of the innermost part of the accretion disk of $R_{in} \approx 3.6 \times 10^9$ cm. This value is consistent with the radius of the WD ($R_{WD} = 5 \times 10^8$ cm) derived by Martinez-Pais et al. (1994). Bisikalo et al. (2008) by using Doppler tomography in SS Cyg in quiescence found $R_{in} = (2.6 - 3.3) \times 10^9$ cm, in agreement with the value derived, with less elaborate mode, by Giovannelli et al. (1983).

From the goodness of Giovannelli et al. (1983) parameters several other results are coming out, like the position of SS Cyg in the plot of the Keplerian period at the surface of the WD, contrary to the position plotted by Patterson (1981), who used the Chandrasekhar limit for the WD mass of SS Cyg (see Fig. 12, left panel). Another interesting results is reported in Fig. 12 (right panel). Indeed, if we use the diagram $\dot{M}_{tr}$ vs R_d (the mean mass-transfer rate vs. radius of the accretion disk) and the critical accretion rate marked with red line in the right panel of Fig. 12 (Schreiber & Lasota, 2007):

$\dot{M}_{crit} = 9.5 \times 10^{15}$ g s$^{-1} \times R_{10}^{2.68} \times M_{WD}$ ($M_\odot$)
(being R_{10} the accretion disk radius in unit of 10^{10} cm),

and the critical accretion rate for SS Cyg derived with the Giovannelli et al. (1983) parameters is:

$\dot{M}_{crit}$(SS Cyg) $= 1.6 \times 10^{17}$ g s^{-1}

Thus, the position of SS Cyg is marked with the light-red rectangle, according to experimental error bars, in the right panel of Fig. 12.

In our opinion, another open question is that about the nature of SS Cyg: NMCV or MCV (IP). There are many papers that discuss such a problem, like those by Giovannelli (1985b, 1996),

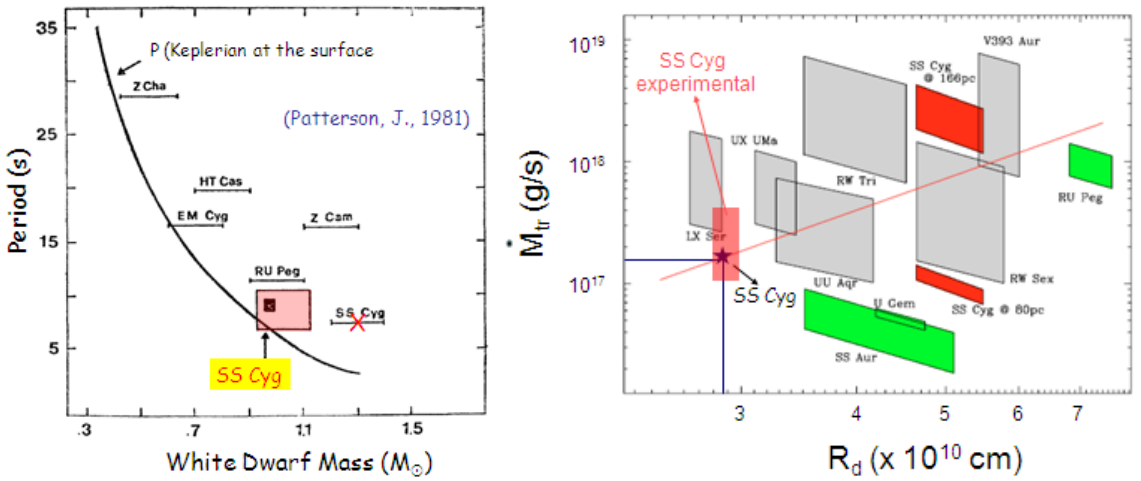

Figure 12: Left panel: Keplerian period at the WD surface versus WD mass (Giovannelli et al., 1983 after Patterson, 1981). Right panel: (adapted from Schreiber & Lasota, 2007).

Name[a]	α, δ[b] (IBIS position)	type[c]	offset[d] (°)	Map code[e]	Count rate[f] (ct s^{-1})	Exposure (ks)	Flux[g] 20-100 keV	P_{orb} (min)	P_{spin} (s)	Distance[h] (pc)	Refs
1RXS J002258.3+614311	5.739,61.714	IP	1.7	B4(8.7)	0.15 ± 0.01	3707	0.81	241.98	503.53	510	[1,2,3,4]
V709 Cas	7.207,59.303	IP	0.8	B5(54.3)	1.03 ± 0.01	3562	5.53	320.4	312.77	300	[1,2,5]
XY Ari*	44.047,19.457	IP	1.1	B5(5.5)	0.53 ± 0.12	119	2.85	363.884	206.298	610	[1,2,6]
GK Per	52.777,43.928	IP/DN	1.7	B5(4.7)	0.26 ± 0.07	277	1.4	2875.4	351.34	-	[1,2]
TV Col*	82.357,-32.819	IP	0.1	B4(11.6)	0.68 ± 0.08	248	0.37	329.181	1911	330	[1,2,7,8]
TW Pic*	83.796,-57.908	IP?/VY Scl?**	2.5	B1(5.8)	0.3 ± 0.07	363	1.61	-	-	-	[1,2,9,10,11]
BY Cam	85.728,60.842	AP	1.2	B5(5.1)	0.69 ± 0.11	162	3.7	201.298	11846.4	140	[1,2]
MU Cam	96.316,73.567	IP	0.6	B4(5.4)	0.24 ± 0.06	548	1.29	283.104	1187.24	440	[1,2,12]
SWIFT J0732.5−1331*	113.13,-13.513	IP	1.6	B3(6.1)	0.39 ± 0.06	409	2.09	336.24	512.42	-	[1,2,13]
V834 Cen	212.260,-45.290	P	0.9	B1(5.4)	0.16 ± 0.03	1675	0.86	101.51712	6091.0272	70	[1,2]
IGR J14536−5522	223.421,-55.394	P	2.0	B4 (11.9)	0.27 ± 0.03	2658	1.45	189.36	11361.6	140	[1,2,14]
NY Lup	237.052,-45.481	IP	0.5	B5(49.1)	1.17 ± 0.03	3141	6.28	591.84	693.01	-	[1,2,15]
V2400 Oph	258.173,-24.279	IP	2.2	B3(33.4)	0.68 ± 0.02	4453	3.65	204.48	927.6	180	[1,2,16]
1H 1726−058	262.606,-5.984	IP	0.7	B5(22.8)	0.85 ± 0.04	1449	4.56	925.27	128	-	[1,2,17]
V2487 Oph	262.968,-19.244	IP/Ne**	2.3	B3(9.1)	0.18 ± 0.02	4562	0.97	-	-	-	[1,2,18]
AX J1832.3−0840*	278.083,-8.721	?	3.1	B4(5.5)	0.07 ± 0.03	3000	0.38	-	-	-	[1,2,19,20]
V1223 Sgr	283.753,-31.153	IP	0.8	B5(52.2)	1.45 ± 0.03	2358	7.79	201.951	746	150	[1,2]
V1432 Aql	295.052,-10.421	AP	0.2	B5(10.8)	0.69 ± 0.07	429	3.7	201.938	12150.4	240	[1,2,21,22]
V2069 Cyg	320.906,42.279	IP*	1.8	B5(6.2)	0.21 ± 0.03	1648	1.13	448.824	743.2	-	[1,2,23,24]
1RXS J213344.1+510725	323.446,51.122	IP	0.3	B5(25.8)	0.65 ± 0.03	2207	3.49	431.568	570.82	-	[1,2,25]
SS Cyg	325.696,43.582	DN	0.6	B5(23.0)	0.7 ± 0.03	1674	3.76	396.3872	-	-	[1,2,26]
FO Aqr	334.514,-8.354	IP	1.7	B4(6.1)	0.65 ± 0.2	54	3.49	290.966	1254.45	250	[1,2,27]
AO Psc*	343.815,-3.194	IP	1.3	B4(4.8)	0.43 ± 0.11	108	2.31	215.461	805.2	200	[1,2,28,29]

Figure 13: List of CVs measured by the INTEGRAL observatory in the hard X-ray range (adapted from Scaringi et al. (2010).

Lombardi, Giovannelli & Gaudenzi (1987), Giovannelli, Martinez-Pais & Sabau-Graziati (1992), Marchev, Kjurkchieva & Ogloza (1999), Gaudenzi et al. (2002), Giovannelli & Sabau-Graziati (1999, 2012a,b). In particular in the latter two papers (2012a,b) a deep discussion of the pro and contra about the IP nature of SS Cyg is reported.

However, since we would like to convince a reader that it is always appropriate to use wisdom in every event of life and in particular in science, I ask a question below to which each one will be able to answer as best he can, however trying to avoid prejudices.

INTEGRAL observatory measured hard X-ray emission from 23 MCVs, with the exception of SS Cyg, classified as NMCV, as shown in Fig. 13 (Scaringi et al., 2010). Thus, our question is: why all the CVs measured by the INTEGRAL are MCVs, but SS Cyg? And, if SS Cyg is NMCV, why INTEGRAL did not measure any other NMCV?

4. Multifrequency behaviour of SS Cyg and its intermediate polar nature

An important behaviour of SS Cyg is known as the UV–optical delay(the delay of the extreme ultraviolet (EUV) flash with respect to the optical flash), which was observed and modeled for cataclysmic variables (e.g. Smak, 1984, 1998; Lasota, 2001).

Figure 14 (upper panel) shows such behaviour: left - Ariel V X-ray data and AAVSO data (Ricketts, King & Raine, 1979), right - hard X-ray. soft X-ray from EXOSAT and AAVSO data (Watson, King & Heise, 1985); lower panel shows RXTE, EUVE and AAVSO delays (Wheatley, Mauche & Mattei, 2003).

Time-lag between HE events and LE events in disk-fed accreting X-ray binaries (XRBs) has been noted in many systems, but the trigger of the work resulted in a model for explaining in general such a phenomenon (Bisnovatyi-Kogan & Giovannelli, 2017) was given by Giovannelli & Sabau-Graziati (2011) who noted a systematic delay between the relative enhancement in luminosity of the optical Be star – occurring at the periastron passage of the neutron star – and the subsequent X-ray flare in the system HDE 245770/A 0535+26. The model for such a system was developed and corroborated by many events (Giovannelli, Bisnovatyi-Kogan & Klepnev, 2013: GBK13), and later by events reported in Giovannelli et al. (2015) where also a relationship between ΔV_{mag} of the optical star at the periastron and X-ray intensity (I_X) of the 8-day delayed flare was produced.

It is right to remind that the mechanism proposed by GBK13 for explaining the X-ray-optical delay in A 0535+26/HDE 245770 is based on an enhanced mass flux propagation through the viscous accretion disk. Time delays have been detected also in several other X-ray transient binaries. This is the reason that urged Bisnovatyi-Kogan & Giovannelli (2017) to generalize the aforementioned model, developed for the particular case of A 0535+26/HDE 245770 (Flavia' star). This general model provides the formula (5) of the time delay between the optical and X-ray flashes appearance in transient cosmic accreting sources:

$$\tau = 6.9 \frac{m^{2/3} \dot{m}^{1/15}}{\alpha^{4/5} (T_4)^{28/15}} \tag{5}$$

where:

$m = M/M_\odot$; $\dot{m} = \dot{M}/(10^{-8}\ M_\odot/yr)$; $T_4 = T_0/10^4$ K ;
α = viscosity , and T_0 = maximum temperature in optics.

By using this formula it is possible to obtain an excellent agreement between the experimental (τ_{exp}) and theoretical (τ_{th}) delays found in:

- X-ray/Be system A0535+26/HDE245770: $\tau_{exp} \simeq 8$ days (GBK13); $\tau_{th} \simeq 8$ days;
- Cataclysmic variable SS Cygni; τ_{exp} = 0.9–1.4 days (Wheatley, Mauche & Mattei, 2003); $\tau_{th} \simeq 1.35$ days;
- Low-mass X-ray binary Aql X-1/V1333 Aql: $\tau_{exp} \sim 3$ days (Shahbaz et al., 1998); $\tau_{th} \simeq$ 3.2days
- Black hole X-ray transient GRO J1655-40: $\tau_{exp} \sim 6$ days (Orosz et al., 1997); $\tau_{th} \simeq 6.5$ days.

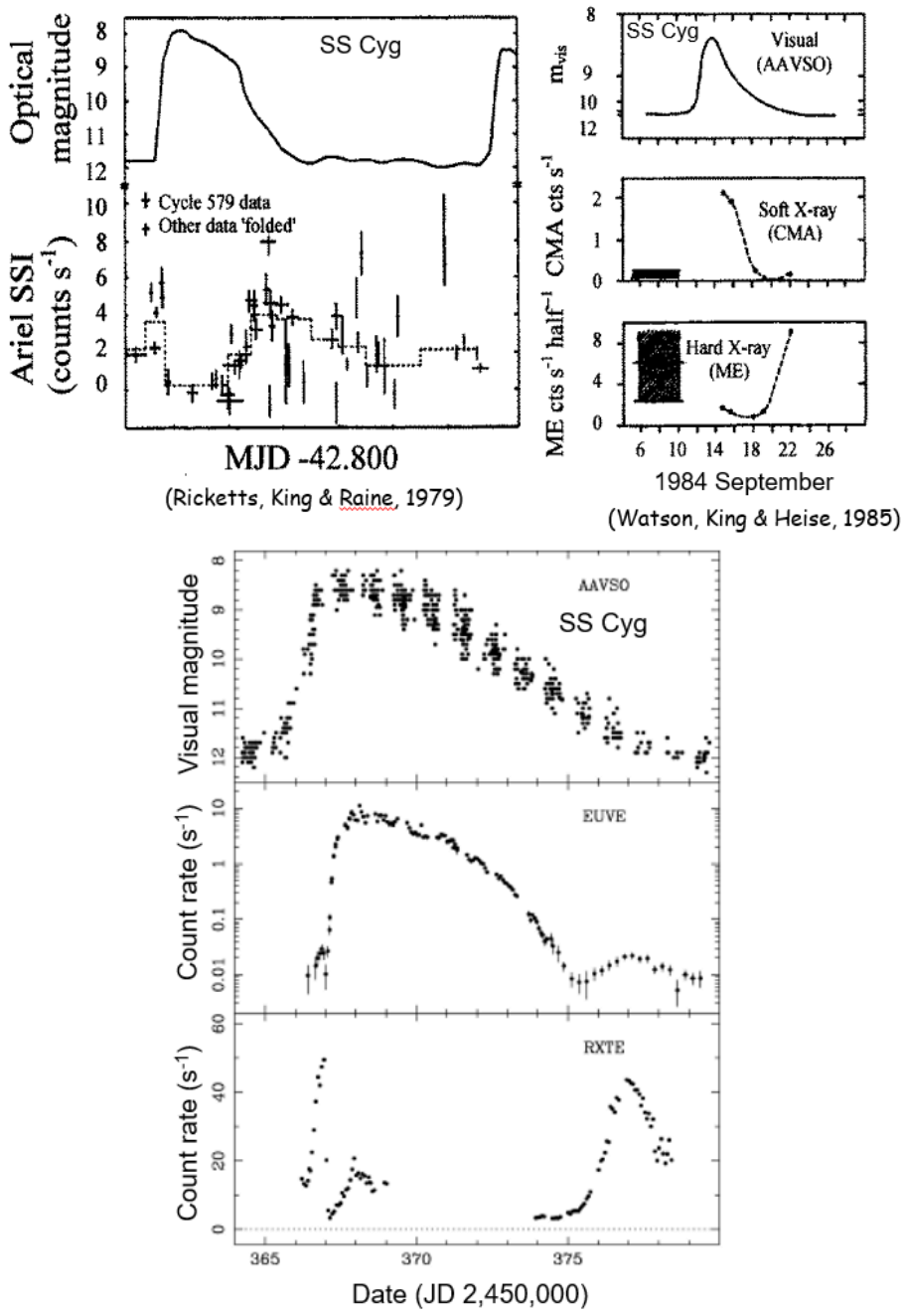

Figure 14: Upper panel: left - Delay between Ariel V X-ray data and Optical AAVSO data (adopted from Ricketts, King & Raine, 1979); right - Hard and soft X-ray data from EXOSAT and Optical AAVSO data (adopted from Watson, King & Heise, 1985). Lower panel: RXTE X-ray, EUVE UV and AAVSO Optical data (adopted from Wheatley, Mauche & Mattei, 2003).

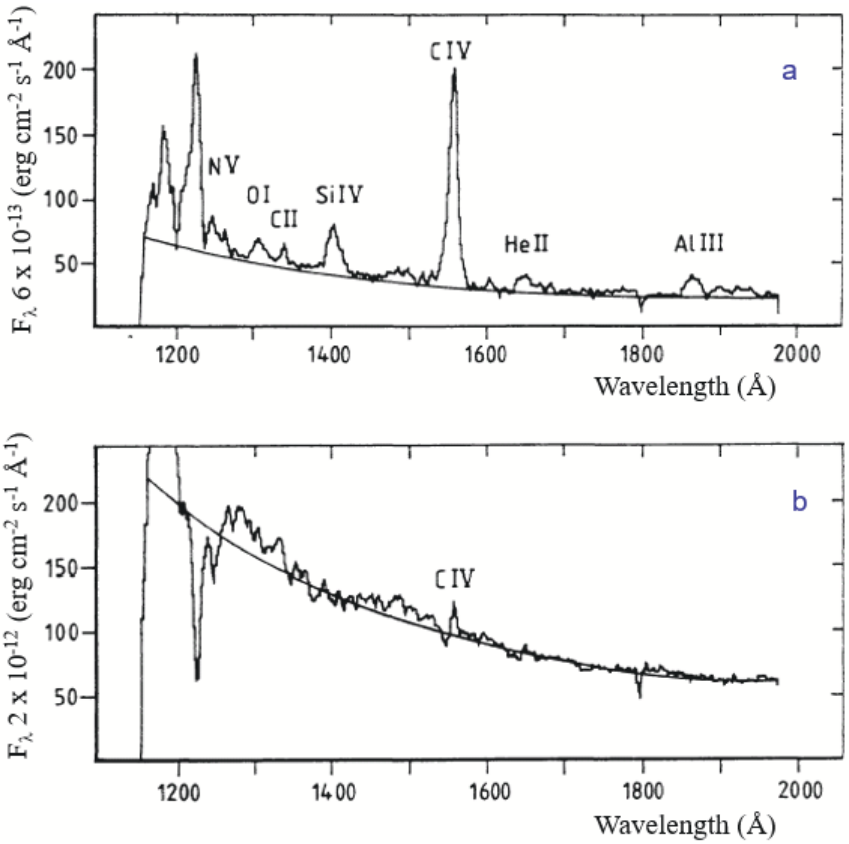

Figure 15: IUE SW-spectra of SS Cyg in quiescence (a) and in outburst (b) (adopted from Giovannelli et al., 1985b).

In this general formula the α-viscosity parameter plays an important role, and usually it is hard to be determined. However, if the other parameters are known, because experimentally determined, the formula (5) can be used for determining α, taking into account the experimental delay measured in a certain source.

SS Cyg has been the subject of numerous observations with the International Ultraviolet Explorer (IUE) in low- and high-resolution mode, many of which were assigned to our group. In the following several important results coming out from those observations.

Figure 15 shows the spectra of SS Cyg in quiescence (a) and outburst (b) in the short wavelength (SW) region (1150 to 2000 Å) (Giovannelli et al., 1985b). The flux $F_\lambda \propto \lambda^\alpha$, being α = -4 for $\lambda \leq$ 1450 Å, and α = -1.2 for $\lambda \geq$ 1450 Å.

It is important to remark that α = -4 is consistent with a tail of a Rayleigh-Jeans emission from a black body (BB) with T $\simeq$ 15 KeV. This slope is the same of that of AM Her: the prototype of POLARS!!!

A cataclysmic variable can be considered as intermediate polar if its magnetic field intensity is of order of 10^6 G and is respecting the following characteristics:

1. Stable optical rotational modulation ($P_{spin} \ll$ Porb).
2. Stable X-ray rotational modulation ($P_{spin} \ll$ Porb).

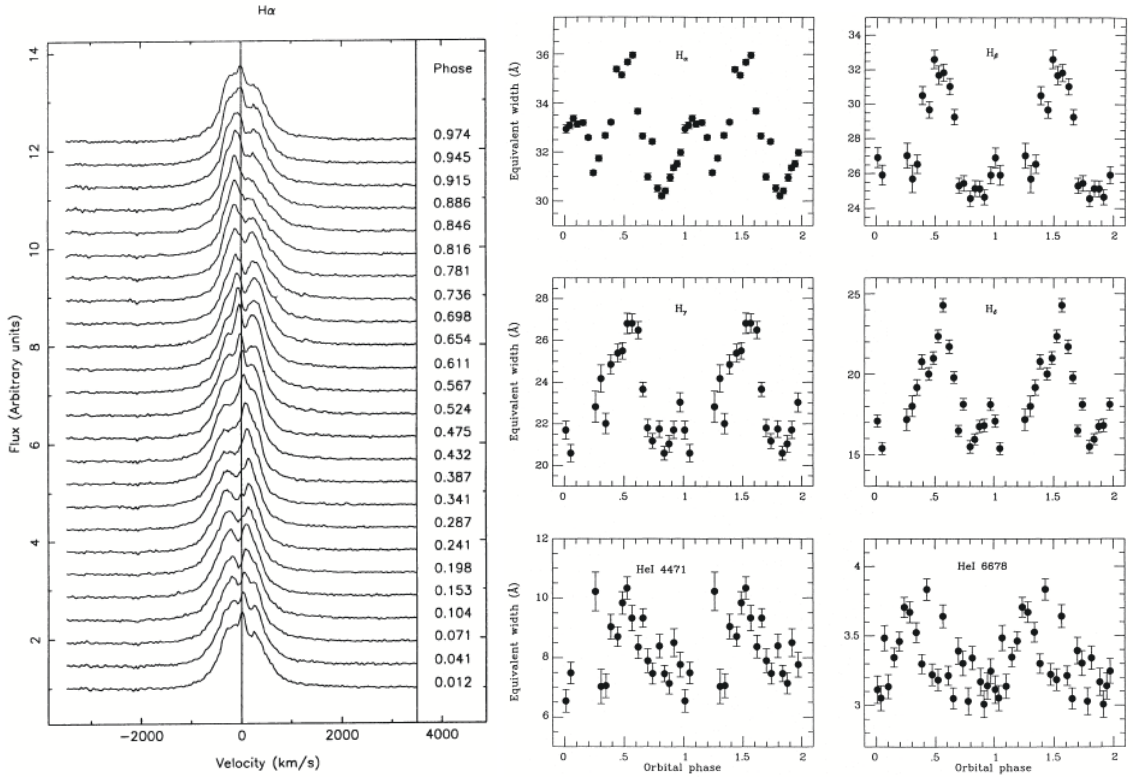

Figure 16: Left panel: Orbital modulation of H_α. Right panel: Orbital modulations of the equivalent widths of H_α, H_β, H_γ, H_δ, HeI (4471 Å), and HeI (6678 Å) (adopted from Martinez-Pais et al., 1994).

3. Emission line flux of HeII orbitally (and rotationally) modulated (due to photoionization caused by the X-ray source).

4. Circular polarization.

5. Modulations at bit periods between P_{spin} and Porb.

6. Very hard X-ray spectrum with strong absorption at low energies.

Points 2 and 4 are fundamental.

Figure 16 shows optical line fluxes orbital modulations: H_α modulation (left panel); the modulation of the equivalent widths of H_α, H_β, H_γ, H_δ, HeI (4471 Å), and HeI (6678 Å) (right panel) (Martinez-Pais et al., 1994).

Left panel of Fig. 17 shows the SS Cyg orbital modulations of the continuum at 1700 Å in quiescence after a long outburst and a short outburst (a) and (b), respectively, and at 2700 Å after a short outburst (c). Central and right panels of Fig. 17 show the SS Cyg orbital modulations in quiescence of the emission lines NV, CIV and SiIV after a short and long outbursts, respectively (Lombardi, Giovannelli & Gaudenzi, 1987).

These orbital modulations have been confirmed by the BVR and BVRI measurements of SS Cyg in quiescence and in outburst, respectively, as shown in Fig. 18 (Kjurkchieva, Marchev & Ogloza, 1998).

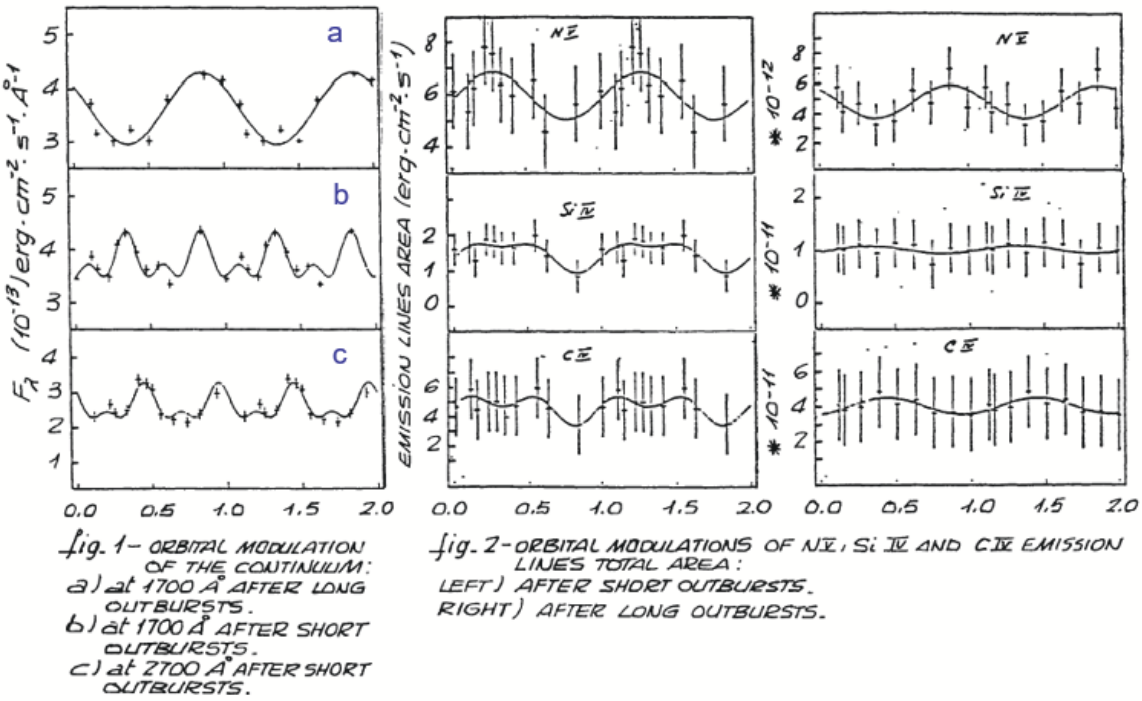

Figure 17: Left panel shows the SS Cyg orbital modulations of the continuum at 1700 Å in quiescence after a long outburst and a short outburst (a) and (b), respectively, and at 2700 Å after a short outburst (c). Central and right panels show the SS Cyg orbital modulations in quiescence of the emission lines NV, CIV and SiIV after a short and long outbursts, respectively (adopted from Lombardi, Giovannelli & Gaudenzi, 1987).

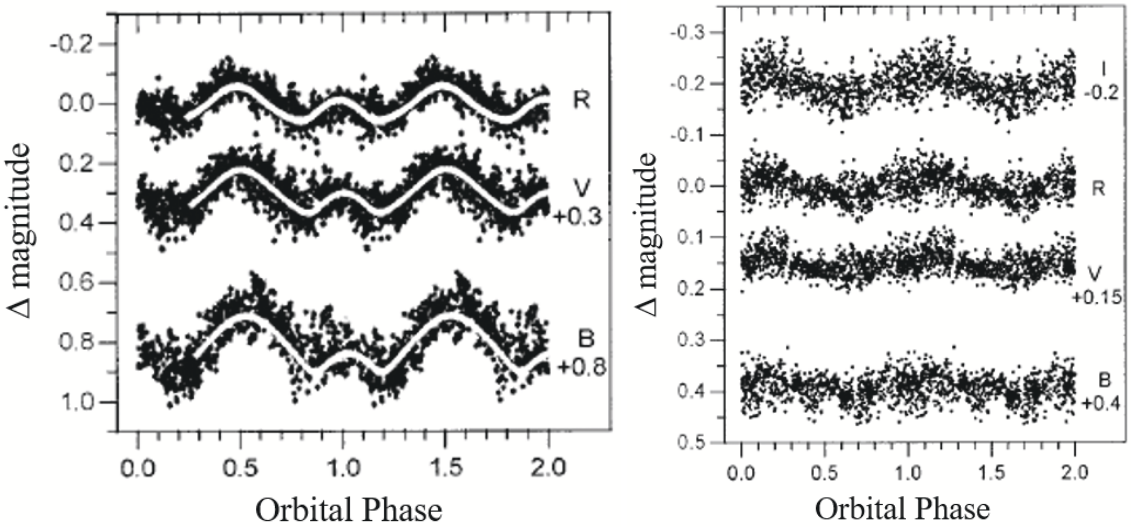

Figure 18: Left panel: BVR orbital modulation of SS Cyg in quiescence. Right panel: BVRI orbital modulation of SS Cyg in outburst (adopted from Kjurkchieva, Marchev & Ogloza, 1998).

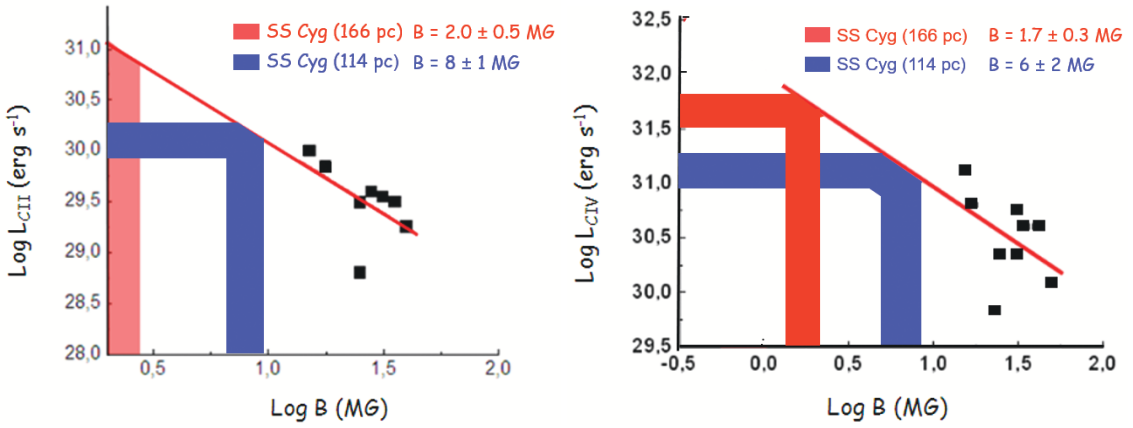

Figure 19: Left panel: CII luminosity vs B. Right panel: CIV luminosity vs B (after Howell et al., 1999). The luminosity of CII and CIV are coming from Gaudenzi et al. (2002).

Thus, we have shown that the continuum of the IUE spectra is similar to that of AM Her. The UV and optical continua and fluxes of emission lines show orbital modulation. Pulsations in hard X-rays during quiescence and in soft X-rays in outbursts are compatible with B $\approx$ 1 MG (e.g. Fabbiano et al., 1981 report B $\lesssim$ 1.9 MG). The rotational period of the WD is $\simeq$ 12 min (Bartolini et al., 1985) is compatible with the IP nature ($P_{spin} \ll P_{orb}$). Dubus et al. (2004) concluded that variations in the mid-IR (11.7 μm) emission could be due to coherent emission during flares. This would probably requires very powerful magnetic field of $\sim 10^7$ G.

So that it is important to determine the magnetic field intensity in the white dwarf of SS Cyg by using all information available. A critical point for this purpose is coming from the indetermination of the distance of SS Cyg: The distance, measured with the Hubble Space Telescope (HST), is D_H = 166 ± 12 pc (Harrison et al., 1999), or using very long baseline interferometric radio observations the distance is D_M = 114 ± 2 pc (Miller-Jones et al., 2013), or D_P = 114.6 ± 0.6 pc (Pala et al., 2020). Howell et al. (1999) found a correlation between the strength of the high-state UV emission lines and the strength of the white dwarf magnetic field, B. By using such a relationships and the luminosity of CII and CIV derived for SS Cyg placed at distance of 166 pc or 114 pc from the fluxes measured with the IUE (Gaudenzi et al., 2002), it is possible to derive the magnetic field intensity of order $2^{+0.5}_{-0.6}$ MG or 6^{+3}_{-2} MG depending on the distance. Figure 19 shows the luminosity of: CII vs B (left panel) and CIV vs B (right panel).

Körding et al. (2008) showed the hardness intensity diagram (HID) for X-ray binaries (XRBs) and SS Cyg. The analogy among black holes, neutron stars and SS Cyg appears evident (left panel of Fig. 20). They detected also a radio jet from SS Cyg (right panel of Fig. 20), and upper limits for linear and circular polarization of 3.2 ± 2.7% and -3.2 ± 2.7%, respectively. They have some difficulties in explaining the behaviour of SS Cyg under the hypothesis that SS Cyg is a dwarf nova. Everything would be better explained if instead SS Cyg were an intermediate polar, as suggested earlier by the analysis of Fig. 19, especially if the distance of SS Cyg was 114 pc instead of 166 pc, so the intensity of the magnetic field would be approximately 6 MG. This value of B would support the expectation of Dubus et al. (2004) to explain the variations in the mid-IR (11.7 μm) emission.

Following the fundamental paper "*Torques and instabilities in intermediate polars*" (Warner,

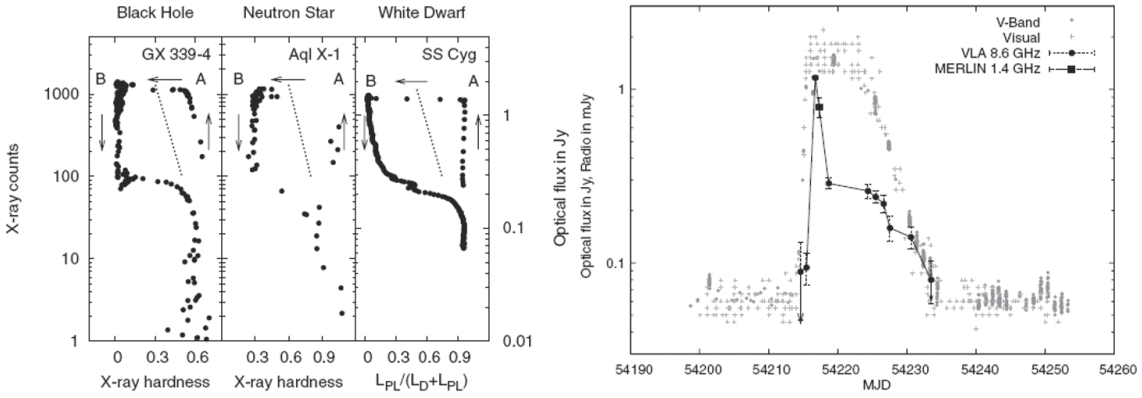

Figure 20: Left panel: Hardness intensity diagrams (HID) for a black hole, a neutron star and the dwarf nova SS Cyg. The arrows indicate the temporal evolution of an outburst. The dotted line indicates the "jet line" observed in black hole and neutron star XRBs: on its right side one generally observes a compact jet; the crossing of this line usually coincides with a radio flare. The hardness ratio for XRBs is defined as the ratio of the counts in the 6.3-10.5 keV range to 3.8–6.3 keV range, and the X-ray counts represent the 3.8–21.2 keV counts of the Rossi X-ray Timing Explorer. For SS Cyg L_D is the disc/boundary layer luminosity derived from the extreme ultra-violet counts. The X-ray luminosity L_{PL} is for the 3-18 keV energy range. Right panel: Radio and optical light-curve of SS Cyg (adopted from Körding et al., 2008).

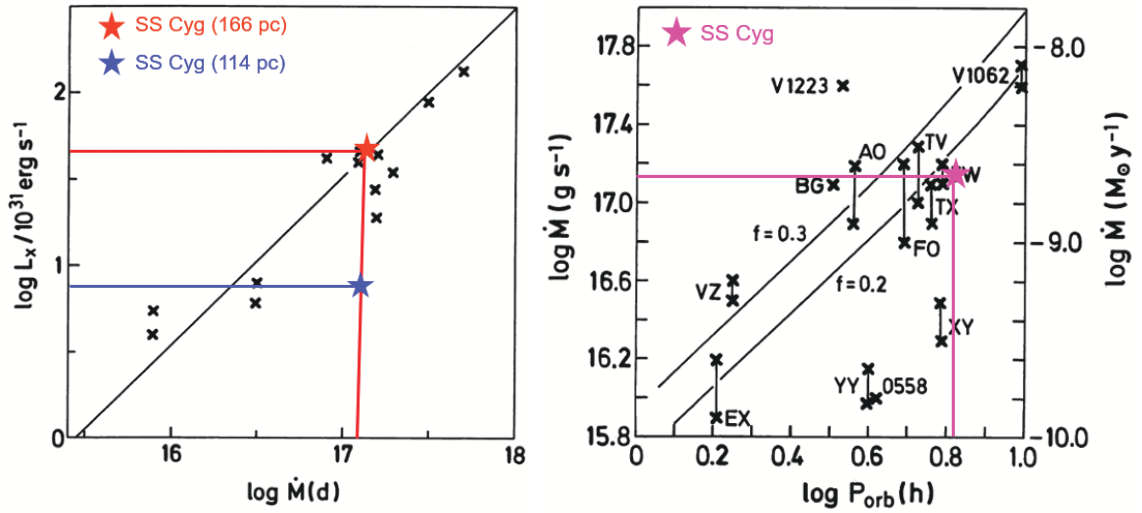

Figure 21: Left panel: Comparison of mass transfer rate and luminosity in 2-10 keV range. Right panel: Intermediate polars in the $\dot{M}$ - P_{orb} plane (adapted from Warner, 1996). SS Cyg position is reported using data from Martinez-Pais et al. (1994) and Hessman et al. (1984).

1996) we want to remark that very probably SS Cyg is an intermediate polar.

Left panel of Fig. 21 shows the relationship between X-ray luminosity (in erg s^{-1}) and accretion rate (in g s^{-1}) onto the white dwarf for IPs. The position of SS Cyg is reported for a distance of 166 pc and 114 pc. Right panel of Fig. 21 shows the relationship between the accretion rate (in g s^{-1}) onto the white dwarf for IPs and orbital period (in hour). The position of SS Cyg is reported too (after Warner, 1996).

Tramontana (2007) using the didactic telescope TACOR of the La Sapienza University of Roma collected 504 images on October 26, 2006 with SS Cygni in outburst. He found P_T = 12.175 ± 0.539 min compatible with Bartolini et al. (1985) value of P_B = 12.18 ± 0.01 min. This periodicity correspond to P_{rot-d} = 11.82 m or P_{rot-i} = 12.56 m if the rotation is direct or inverse with the orbital motion, respectively. Braga (2009) using 10,000 s UV data from XMM-OM found P_{rot-Br} = 709 ± 1 s corresponding to P_{rot-Br} = 11.82 ± 0.02 m.

P_T, P_B, and P_{rot-Br} stand for the periods found by Taverna, Bartolini and Braga, respectively.

Thus, in Table 1 we show the characteristics parameters of EI UMa – a well established IP (Reimer et al, 2008) – and those of SS Cyg.

The unbiased reader will have to explain why EI UMa is an IP and SS Cyg is not!

Table 1: Comparison of the characteristic parameters of EI UMa – a well established IP (Reimer et al., 2008) – and SS Cyg (Giovannelli et al., 1983; Lombardi, Giovannelli & Gaudenzi, 1987; Gaudenzi et al., 1990, 2002; Giovannelli & Martinez-Pais, 1991; Schreiber & Gänsicke, 2002).

EI UMa	SS Cyg
P_{orb} = 6.434 h	P_{orb} = 6.603 h
P_{opt} = 745 s (~ P_{XMM})	P_{opt} = 709 s (~ $P_{XMM\ UV}$)
0.81 $M_\odot$ < M_{WD} < 1.2 $M_\odot$	M_{WD} = 0.97 $M_\odot$
$R_{WD} = 7 \times 10^8$ cm	$R_{WD} = 5 \times 10^8$ cm
M_R = 0.81 $M_\odot$	M_R = 0.56 $M_\odot$
R_R = 0.76 $R_\odot$	R_R = 0.68 $R_\odot$
$L_X \sim 10 \times 10^{32}$ erg s^{-1}	$L_X \sim (6.6 - 9.8) \times 10^{32}$ erg s^{-1}
$\dot{M} = 3.6 \times 10^{17}$ g s^{-1}	$\dot{M} \simeq (1 - 4) \times 10^{17}$ g s^{-1}
M_V = 5.4	M_V = 5.9
f = Rd/a = 0.2 – 0.3	f = Rd/a = 0.2
UBV Orbital modulations of continuum	UBV & UV Orbital modulations of continuum & emission lines EWs

Figure 22 shows the position of SS Cyg in the plane $P_{spin} - P_{orb}$, being P_{spin} the rotational period of the white dwarf: left panel from Warner (1996); right panel from Norton, Wynn & Somerscales (2004). The P_{spin}/P_{orb} ratio for SS Cyg is ≈ 0.03.

Searches for X-ray periodicities have been performed with GINGA by Ponman et al. (1995). Negative results have been reported for periods around 9 s and 12 min; but we recall that these observations were performed during an outburst phase, while Bartolini et al (1985) measurements – which detected a 12.18 m periodicity – were performed during a quiescent phase of SS Cyg. After the long discussion we have reported in this section we can assume with reasonable certainty that SS Cyg is an IP. However, in order to prove the IP nature of SS Cyg, we took it upon ourselves to analyse a discrete sample of IUE spectra, many from our own observations in search of rotational

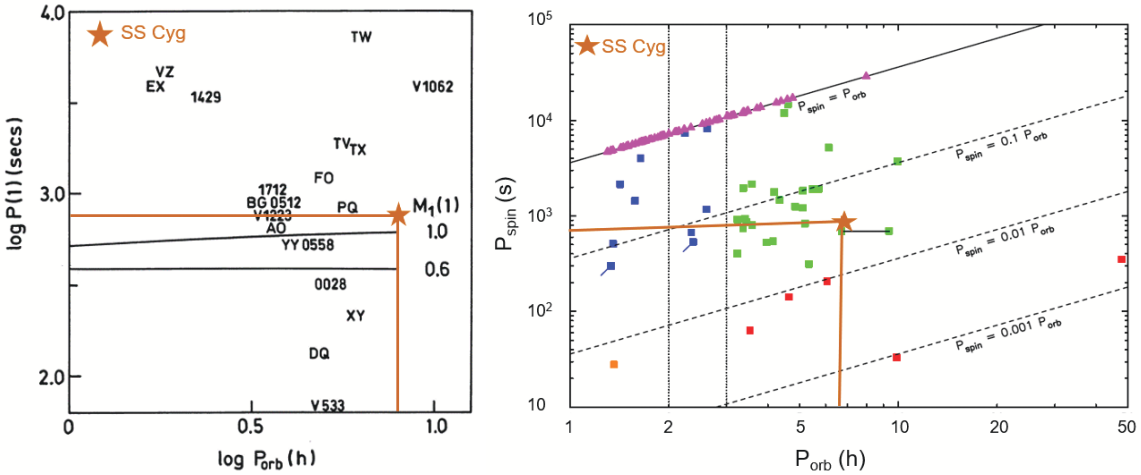

Figure 22: Left panel: The position of SS Cyg in the plane P_{spin} – P_{orb} (adapted from Warner, 1996). Right panel: The position of SS Cyg in the plane P_{spin} – P_{orb} (adapted from Norton, Wynn & Somerscales, 2004). P_{spin} is the rotational period of the white dwarf.

periodicity.

5. IUE observations of SS Cyg

The sample is formed by 36 low resolution short wavelength spectra during quiescence obtained in different observational runs performed with the IUE between 1978 and 1990. The journal of observations is shown in Fig. 23 together with the emission lines fluxes.

From columns 1 to 5 the numbers of the image, the heliocentric JD - corresponding to the middle exposure -, the exposure times, the orbital phase by Hessman et al. (1984) and the m_{FES} magnitude (see Holm and Rice, 1981) are indicated. From column 6 to 10 the emission line fluxes of different ions are shown. The data have been corrected for the instrumental effects by using the standard software developed for IUE data while the data analysis was done by using the IRAF software.

5.1 The time series analysis

A Fourier power spectral analysis has been performed by using the Discrete Fourier Transform (DFT) algorithm of Deeming (1975) for the intensity of the NV (1240.0 Å), CII (1335.1 Å), Si IV (1393.7 – 1402.7 Å), C IV (1548.2 – 1550.8 Å), Al III (1854.7 – 1862.8 Å) emission lines. As it is well known the power spectrum resulting from this technique depends on the particular sampling of the data sequence.

In order to overcome this difficulty the data have been also analyzed with the spectral window deconvolution method (CLEAN) by Roberts, Lehar & Dreher (1987).

Both procedures have been successively applied to each spectral line fluxes data set.

Particular attention was devoted to the choice of the frequency range: the minimum frequency for which spectral information can be obtained is roughly that one corresponding to the total length T of the data span: $\nu_{\min} \approx 1/T$.

Image	HJD +2440000 (day)	Exp. Time (m)	ϕ_h	m_{FES} (mag)	Emission lines Fluxes NV (1240 Å)	CII (1335 Å)	SiIV (1398 Å)	CIV (1549 Å)	AlIII (1859 Å)
							$\times 10^{-13}$ erg cm^{-2} s^{-1}		
SWP03880	3884.9198	16	0.8284	11.92	19.0± 2.0	16.0± 2.0	42.0± 4.0	143.0± 4.0	14.0± 2.0
SWP03881	3884.9628	16	0.9849	11.88	24.0± 4.0	22.0± 5.0	67.0± 7.0	175.0± 6.0	22.0± 3.0
SWP03882	3885.0024	16	0.1287	11.92	30.0± 5.0	23.0± 4.0	64.0± 5.0	207.0± 9.0	24.0± 3.0
SWP03883	3885.0455	16	0.2852	11.87	16.0± 4.0	14.0± 3.0	49.0± 5.0	154.0± 6.0	16.0± 3.0
SWP03884	3885.1031	40	0.4947	11.87	15.0± 4.0	13.0± 3.0	44.0± 4.0	136.0± 5.0	13.0± 2.0
SWP03885	3885.1482	16	0.6588	11.92	22.0± 4.0	19.0± 4.0	51.0± 6.0	166.0± 6.0	18.0± 3.0
SWP05263	4010.8742	16	0.6286	11.90	19.0± 4.0	18.0± 2.0	46.0± 5.0	161.0± 6.0	21.0± 3.0
SWP05264	4010.9044	21	0.7384	11.92*	18.0± 5.0	17.0± 5.0	44.0± 5.0	141.0± 6.0	18.0± 3.0
SWP05265	4010.9381	24	0.8608	11.90*	16.0± 3.0	16.0± 5.0	59.0± 5.0	176.0± 5.0	19.0± 3.0
SWP05266	4010.9715	24	0.9820	11.90*	14.0± 4.0	18.0± 4.0	55.0± 5.0	155.0± 5.0	21.0± 3.0
SWP05267	4011.0055	24	0.1057	11.90*	30.0± 6.0	17.0± 4.0	49.0± 5.0	154.0± 5.0	14.0± 2.0
SWP05268	4011.0388	24	0.2268	11.90*	8.0± 2.0	16.0± 4.0	44.0± 5.0	137.0± 5.0	16.0± 3.0
SWP05269	4011.0729	24	0.3505	11.90*	24.0± 4.0	16.0± 4.0	49.0± 5.0	150.0± 5.0	19.0± 3.0
SWP05270	4011.1069	24	0.4742	11.90*	20.0± 4.0	17.0± 3.0	44.0± 5.0	129.0± 5.0	18.0± 3.0
SWP17387	5159.5682	40	0.7282	11.70	29.0± 4.0	20.0± 3.0	72.0± 4.0	214.0± 6.0	21.0± 3.0
SWP17388	5159.6158	25	0.9011	11.83	25.0± 4.0	22.0± 3.0	72.0± 5.0	177.0± 5.0	21.0± 3.0
SWP17414	5163.5896	25	0.3445	11.68	27.0± 4.0	20.0± 3.0	63.0± 7.0	199.0± 7.0	23.0± 3.0
SWP17415	5163.6365	40	0.5149	11.79	29.0± 4.0	21.0± 3.0	77.0± 5.0	190.0± 4.0	21.0± 2.0
SWP29929	6786.0918	20	0.5704	11.82	13.0± 3.0	11.0± 4.0	26.0± 4.0	85.0± 4.0	9.0± 2.0
SWP29930	6786.1474	40	0.7723	11.86	16.0± 4.0	11.0± 3.0	33.0± 4.0	115.0± 5.0	11.0± 2.0
SWP29931	6786.1946	16	0.9440	11.98	14.0± 3.0	10.0± 3.0	29.0± 5.0	105.0± 7.0	10.0± 2.0
SWP30078	6807.8541	35	0.6687	11.75	4.0± 3.0	9.0± 4.0	18.0± 5.0	64.0 ± 7.0	5.0 ± 3.0
SWP30079	6807.9055	35	0.7508	11.80	6.0± 2.0	13.0± 2.0	17.0± 4.0	71.0 ± 5.0	4.0 ± 2.0
SWP30080	6807.9486	15	0.9325	11.86		10.0± 3.0		88.0 ± 6.0	8.0 ± 2.0
SWP30135	6816.9880	40	0.0120	12.03	6.0± 3.0	9.0± 2.0	17.0± 3.0	76.0 ± 5.0	6.0 ± 3.0
SWP30136	6817.0422	40	0.1487	11.94	7.0± 2.0	6.0± 2.0	21.0± 5.0	83.0 ± 5.0	9.0 ± 2.0
SWP30137	6817.0984	40	0.2156	11.96	11.0± 3.0	10.0± 2.0	30.0± 4.0	90.0 ± 5.0	8.0 ± 2.0
SWP37866	7881.9682	40	0.6056	12.04	11.0± 2.0	10.0± 1.0	21.0± 3.0	90.0± 10.	0 5.0± 0.7
SWP37867	7882.0272	40	0.7847	12.21	9.0± 1.0	12.0± 2.0	29.0± 4.0	120.0± 20.	0 6.0± 0.9
SWP37868	7882.0824	35	0.0043	11.97	9.0± 1.0	11.0± 2.0	27.0± 4.0	120.0± 20.	0 7.0± 1.0
SWP37869	7882.1331	35	0.2958	12.09	13.0± 2.0	16.0± 2.0	29.0± 4.0	120.0± 20.	0 9.0± 1.0
SWP37870	7882.1866	35	0.4902	12.04	8.0± 1.0	10.0± 1.0	25.0± 4.0	90.0± 10.	0 8.0± 1.0
SWP37924	7891.9627	40	0.0231	12.10	10.0± 1.0	7.0± 1.0	17.0± 2.0	80.0± 10.	0 6.0± 0.9
SWP37925	7892.0190	42	0.2275	12.22	6.0± 1.0	11.0± 2.0	16.0± 2.0	80.0± 10.	0 6.0± 0.9
SWP37926	7892.0752	40	0.4320	12.17	13.0± 1.0	9.0± 1.0	19.0± 3.0	90.0± 10.	0 7.0± 1.0
SWP37927	7892.1322	40	0.6389	12.09	9.0± 1.0	9.0± 1.0	16.0± 2.0	80.0± 10.	0 6.0± 0.9

Figure 23: Journal of observations: the values of m_{FES} magnitude marked with * are not obtained by FES counts but from VILSPA log – book

The maximum frequency deserves a more careful discussion: in the case of constant sampling rate Δ, the Nyquist frequency (Shannon 1949) $\nu_N = 1/(2\Delta)$, is the highest for which information can be retrieved.

For randomly distributed data, where Δ_{min} is the smallest spacing between two successive data, the frequency $\nu = 1/(2\Delta_{min})$, is generally considered as ν_{max} (Scargle,1982).

Nevertheless, the work of Roberts, Lehar & Dreher (1987) on synthetic unevenly spaced time series shown that it is possible to retrieve significant information also on frequencies higher than ν_{max} by means of a cleaning procedure of the "DIRTY" spectrum.
From our data set we can infer a theoretical frequency resolution $\Delta\nu \approx 1/T = 2.5\times10^{-4}\ cycle/day$ and a maximum frequency $\nu_{max} = 16.7\ cycle/day$.
Our DIRTY spectra obtained are shown in Figure 24. From these spectra a clear feature at a frequency $\nu_{peak} = 124.57\ cycle/day$ ($11^m.56$) is evident together with the typical features of sampling for sparse data.

For each DIRTY power spectrum we evaluated the signal to noise ratio in an frequency interval centered on ν_{peak}. Successively we evaluated the *false alarm* probability (Scargle 1982, Horne and Baliunas, 1986). The *false alarm* probability F tells us the probability to have a peak of height z

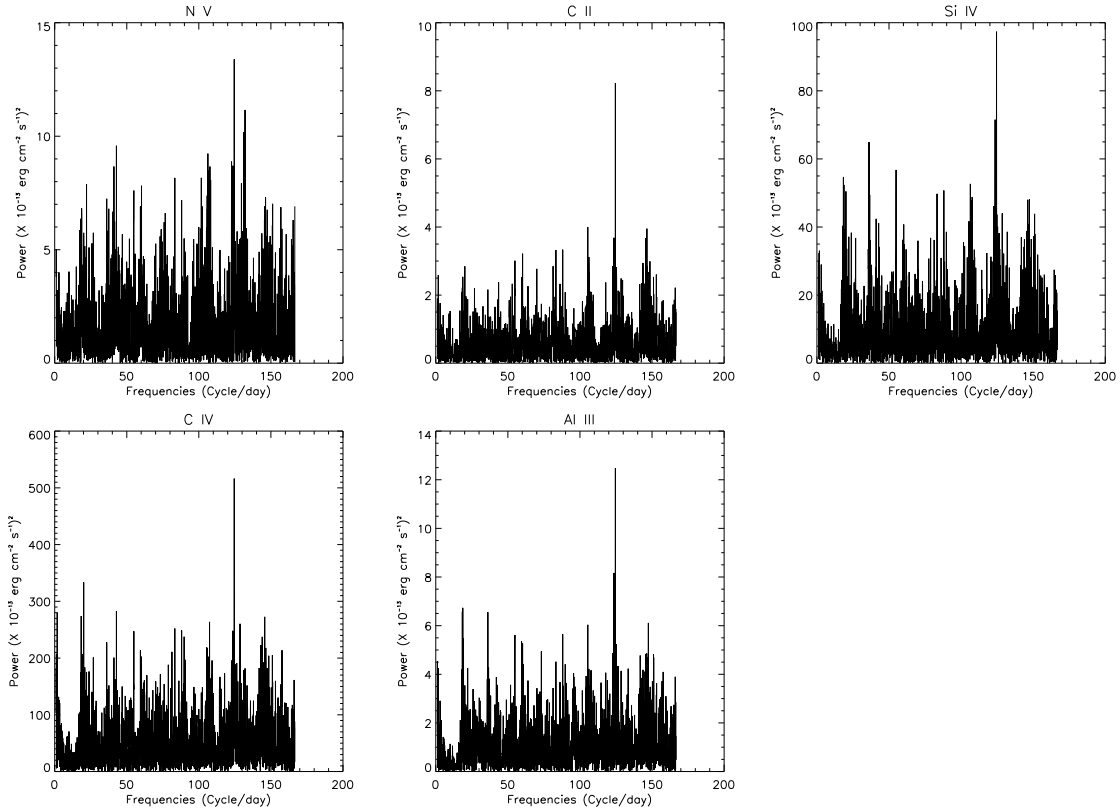

Figure 24: The power spectra obtained by utilizing DFT. The frequency at $\nu = 124.57\ cycle/day$ ($11^m.56$) is clearly visible for each ion.

Ion	S/N	F	1-F
NV	6.5	0.050	95%
CII	9.9	0.002	>99%
SiIV	7.9	0.013	99%
CIV	8.5	0.007	>99%
AlIII	9.1	0.004	>99%

Table 2: The S/N ratio, the value of the *False Alarm* probability and the confidence level associated with the indicated ions periodgrams (see text)

or higher assuming that the data are *pure noise*. So the probability that the data contain a signal is given by $1 - F$. All these quantities are summarized in Table 2.

As it is possible to see in Table 2, with the exception of NV, the S/N ratio of the signal in the power spectrum is high. The value of the *false alarm* probability (Scargle 1982) indicates that the pulsation at $\nu_{\rm peak}$, with a confidence level of 99% is a true signal.

The periodicity found on our DIRTY spectra being very close to the I–R periodicity found by Bartolini et al. (1985), we applied the CLEAN procedure to the data with a gain value of 0.1 and a

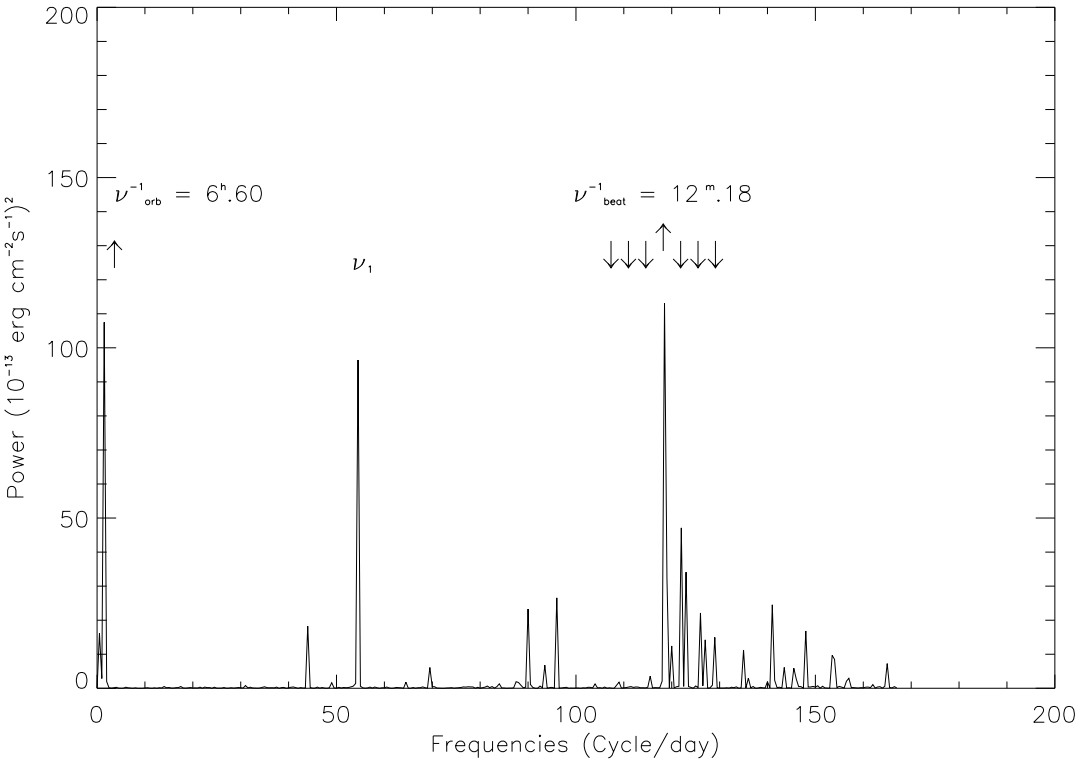

Figure 25: The cleaned spectrum for the CIV data is shown. ↑ indicates the $\nu_{\rm orb}$ and $\nu_{\rm beat}$ while the other arrows the $\nu_{\rm beat} \pm K\nu_{\rm orb}$ harmonics.

number of iterations of the CLEAN algorithm from 500 to 1000, depending on the line.
Figure 25 shows as example the cleaned spectrum for the C IV data set. In this figure the frequency $\nu_{\rm orb} = 3.63\ \ cycle/day$ at the orbital period $P_{\rm orb} = 0^d.27512973$ (Martinez–Pais et al. 1994), and the frequency $\nu_{\rm beat}$ at the beat period $P_{\rm beat} = 12^m.18$ found by Bartolini et al. (1985) from I – R photometrical data are marked. The periodicity at $\nu_{\rm beat} \pm K\nu_{\rm orb}$ with $K = 0, 1, 2, 3$ are also indicated.

As it is possible to see by comparing Figs 24 and 25, the peak at frequency 124.57 $cycle/day$ after the deconvolution with the spectral window has a power lower than in the correspondent DIRTY spectrum. On the other hand the deconvolution points out better the $\nu_{\rm beat}$ peak.
The periodicities highlighted from the cleaned power spectra are close to the orbital period of SS Cygni and at the $12^m.18$. Another strong peak is found at $\nu_1 = 54.50\ \ cycle/day$. This peak and the orbital period peak disappear once we subtract the orbital period frequency from the data set. The harmonic subtraction was performed utilizing the Ferraz – Mello (1981) methods.

5.2 Discussion

The $12^m.18$ periodicity is shorter than the average exposure time of the IUE spectra.
This would be a problem for a process with a generic periodic dependence on the time. In fact an integration over a time longer than the period of the process causes the lost of the periodicity since

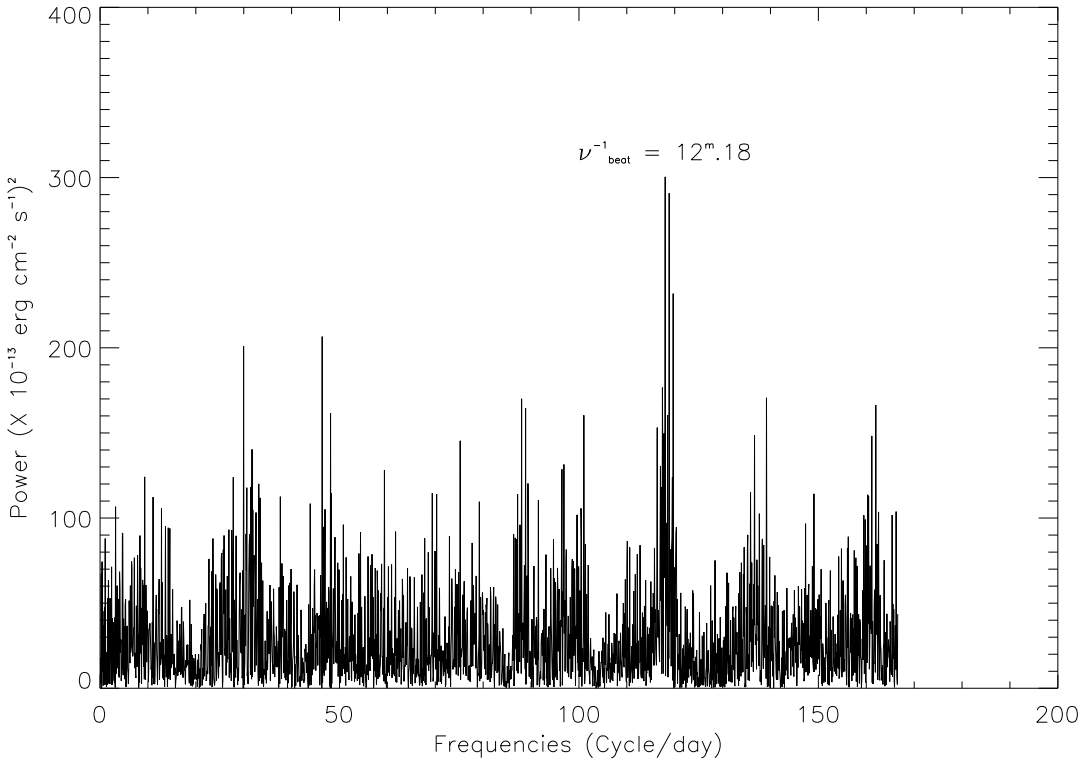

Figure 26: The power spectrum (DFT) of the synthetic time series. The $\nu_{beat} = 12^m.18$ is clearly evident (see text).

the mean value over the period is different by zero.
On the contrary, if the process is time dependent as an alternate or, more strictly, as a sinusoidal function, we have that the integral over the period or an integer multiple of it is zero. The integral over the residual time is different from zero. The barycenter relative to the last time integration interval is different by the true barycenter of the whole integration interval. So the only actual effect is a phase shift depending on the exposition time of the i-th term in the time series.
The high signal to noise ratio and the high confidence levels obtained (see Table 2) make us confident that the $\nu_{\rm peak}$ pulsation indicates at least an alternate signal.
In order to verify the utilized procedure, we performed DFT from synthetic time series. We made simulations of the observations with sinusoidal signals having the same characteristics of our data set, namely: a periodicity equal to $\nu^{-1}_{\rm beat}$; time intervals of the simulated data equal to those of the experimental data; the average exposure time of the simulated observations equal to the experimental average ($29^m.0$).

For these simulations a gaussian relative error of 10% (order of magnitude of the experimental errors) has been introduced. While for equally spaced data it is impossible to distinguish a real periodicity, surprisingly in the unevenly spaced synthetic time series the peak at $\nu_{\rm beat}$ frequency is clearly evident (see Fig. 26).

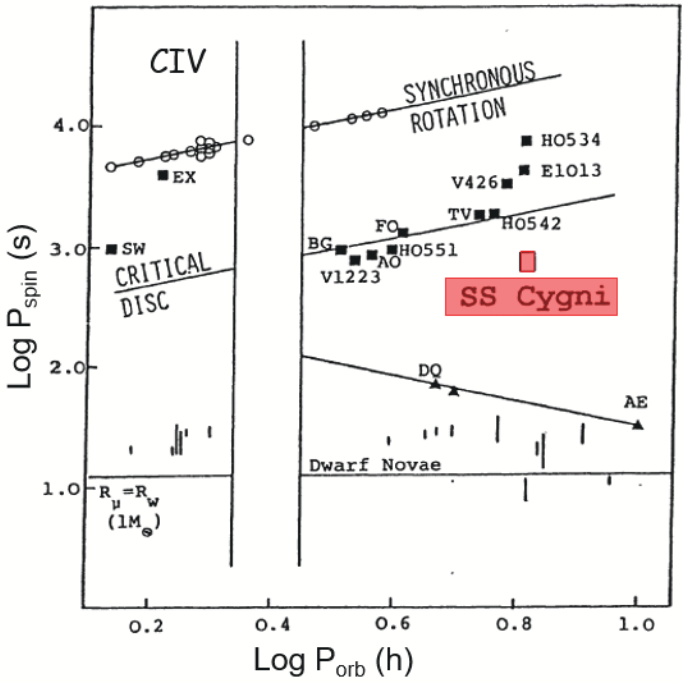

Figure 27: Relationship between spin period P_{spin} and orbital period, P_{orb}, for polars (synchronous rotation), intermediate polars (critical disc), DQ Herculis stars and Dwarf Novae (short vertical bars). The position of SS Cyg is marked with a red square (adapted from Warner & Wickramasinghe, 1991).

6. Conclusions

The Fourier spectral analysis of the emission line fluxes in the UV spectra of SS Cygni in quiescence leads to the following conclusions:

1. The UV data show unambiguously the existence of the $12^m.18$ periodicity found by Bartolini et al. (1985) in the I – R bands during quiescence.

2. The periodicity detected is very coherent. If this periodicity would not be strictly coherent it should be impossible to detect it with exposure times greater than the periodicity itself.

3. It was possible to detect such a periodicity since the observations range on a long time scale with very different time intervals between them and very different exposure times.

4. This result is another experimental evidence that adds to all others indicated in Giovannelli & Martinez–Pais (1991) and favours the intermediate polar (IP) hypothesis in explaining the behavior of SS Cyg. Moreover, the obtained periodicity locates SS Cyg very close to the zone of the IPs above the orbital period gap as shown in Fig. 27 (Warner & Wickramasinghe, 1991).

5. All these four points combined with the results illustrated in Figures 8, 15, 16, 17, 18 19, 20, 21, 22 and in Table 2 demonstrate unequivocally that the nature of SS Cyg is that of an intermediate polar. If sometimes appear that it is not, it means that we are only looking at some details of his behavior.

In particular the multi-periodic behavior of the emission from the system in the X-ray and optical ranges (Cordova et al., 1980, 1984, Patterson, 1981, Giovannelli and Martinez-Pais, 1991), and the supposed presence of a "moderate" magnetic field in the system (Ricketts et al. 1979, Cordova et al. 1980, Szkody, Michalsky & Stokes, 1982, Giovannelli et al., 1985, Claudi 1986, Giovannelli et al. 1990) support this last consideration. If this is the case an X-ray period of $12^m.56$ (retrograde motion) or a period of $11^m.82$ (direct motion) should be present. Up today no such X-ray period for SS Cyg has been detected: during outbursts negative results have been obtained, as could be expected (Ponman et al, 1995); during quiescence phases, the lack of measurements long enough, prevented till now statistical analysis from be performed. Therefore either a re-examination of old X-ray data and/or new X-ray observations are needed in order to have a further and final confirmation of this periodicity.

Acknowledgments: This research has made use of the NASA's Astrophysics Data System.

References

[1] Ak, T., Ozkan, M.T., Mattei, J.A.: 2002, A&A 389, 478-484.

[2] Bath, G.T., van Paradijs, J.: 1983, Nature, 305, 33.

[3] Bartolini, C.,Guarnieri, A., Lolli, M., Piccioni A., Giovannelli F., Gaudenzi S., Lombardi, R.: 1985, in *Multifrequency Behaviour of Galactic Accreting Sources*, F. Giovannelli (Ed.), SIDEREA, Roma, pp. 50-56.

[4] Bisikalo, D.V., Kononov, D.A., Kaigorodov, P.V., Zhilkin, A.G., Boyarchuk, A.A.: 2008, ARep 52, 318-326.

[5] Bisikalo, D.V., Zhilkin, A.G.: 2015, Acta Polytechnica CTU Proc. 2(1), 60–65.

[6] Bisnovatyi-Kogan, G.S., Giovannelli, G.: 2017, A&A 599, A55, 7 pp.

[7] Braga, V.F.: 2009, Thesis in Physics, University La Sapienza, Roma.

[8] Cannizzo, J.K., Mattei, J.A.: 1992, ApJ 401, 642-653.

[9] Claudi, R.U.: 1986, Thesis in Physics, University La Sapienza, Roma.

[10] Cordova, F.A., Chester, T.J., Tuohy, I.R., Garmire, G.P.: 1980, ApJ 235, 163-176.

[11] Cordova, F.A., Chester, T.J., Mason, K.O., Kahn, S.M., Garmire, G.P.: 1984, ApJ 278, 739-753.

[12] Cordova F.A, Nugent J.J., Klein S.R., Garmire G.P., 1980, MNRAS 190, 87-

[13] Deeming T.J.: 1975, Ap&SS, 36, Issue 1, 137-158.

[14] Dubus, G., Campbell, R., Kern, B., Taam, R.E., Spruit, H.C.: 2004, MNRAS 349, Issue 3, 869-881.

[15] Fabbiano, G., Hartmann, L., Raymond, J., Steiner, J., Branduardi-Raymond, G., Matilsky, T.: 1981, ApJ 243, 911-925.

[16] Ferraz-Mello, S.: 1981, AJ 86, 619-624.

[17] Gaudenzi S., Giovannelli F., Lombardi R., Claudi R.: 1990, AcA, 40, 105-115.

[18] Gaudenzi, S., Claudi, R.U., Giovannelli, F., Lombardi, R., Pelosi, M., Strappolini, M.: 2002, Mem. SAIt 73, 213-222.

[19] Giovannelli, F.: 1981, SSRv 30, Issue 1-4, 213-219.

[20] Giovannelli, F. (Ed.): 1985a, *Multifrequency of Accreting Galactic Sources*, SIDEREA, Roma, 371 pp.

[21] Giovannelli, F.: 1985b, in *Multifrequency Behaviour of Galactic Accreting Sources*, F. Giovannelli (Ed.), SIDEREA, Roma, p. 37.

[22] Giovannelli, F.: 1996, in *Multifrequency Behaviour of High Energy Cosmic Sources*, F. Giovannelli & L. Sabau-Graziati (Eds.), Mem. S.A.It., 67, 401-413.

[23] Giovannelli, F.: 2017, in *The Golden Age of Cataclysmic Variables and Related Objects – IV*, Online at https://pos.sissa.it/cgi-bin/reader/conf.cgi?confid=315, id. 1.

[24] Giovannelli, F.: 2021, in *The Golden Age of Cataclysmic Variables and Related Objects – V*, Online at https://pos.sissa.it/cgi-bin/reader/conf.cgi?confid=368, id. 1.

[25] Giovannelli, F., Gaudenzi, S., Rossi, C., Piccioni, A.:1983, AcA 33, 319-329.

[26] Giovannelli, F., Martinez-Pais, I.G., Gaudenzi, S., Lombardi, R., Rossi, C., Claudi, R.U.: 1990, Ap&SS, 169, 125-132.

[27] Giovannelli, F., Martinez-Pais, I.G.: 1991, Space Sci. Rev. 56, 313-372.

[28] Giovannelli, F., Martinez-Pals, I.G., Sabau-Graziati, L.: 1992, in *Viña del Mar Workshop on Cataclysmic Variable Stars*, Nikolaus Vogt (Ed.), ASP Conf. Ser. 29, 119-124.

[29] Giovannelli, F., Sabau-Graziati, L.: 1999, Mem. SAIt 70, 527-546.

[30] Giovannelli, F., Sabau-Graziati, L.: 2011, Acta Polytechnica Vol. 51, No. 2., 21-32.

[31] Giovannelli, F., Sabau-Graziati, L.: 2012a, in *The Golden Age of Cataclysmic Variables and Related Objects*, F. Giovannelli & L. Sabau-Graziati (eds.), Mem. S.A.It., 83 N. 2, 698.

[32] Giovannelli, F., Sabau-Graziati, L.: 2012b, in *Second Workshop on Robotic Autonomous Observatories*, S. Guziy, S.B. Pandey, J.C. Tello & A.J. Castro-Tirado (Eds.), Astronomical Society of India Conf. Ser. 7, 59-78.

[33] Giovannelli, F., Bisnovatyi-Kogan, G.S., Klepnev, A.S.: 2013, A&A 560, id.A1, 11 pp (GBK13).

[34] Giovannelli, F., Bisnovatyi-Kogan, G.S., Bruni, I., Corfini, G., Martinelli, F., Rossi, C.: 2015a, AcA 65, 107-116.

[35] Harrison, T.E., McNamara, B.J., Szkody, P., McArthur, B.E., Benedict, G.F., Klemola, A.R., Gilliland, R.L.: 1999, ApJ 515, Issue 2, L93-L96.

[36] Hartle, J.B., Thorne, K.S.: 1968, ApJ 153, 807-834.

[37] Hessman, F.V., Robinson, E.L., Nather, R.E., Zhang, E.-H.: 1984, ApJ 286, 747-759.

[38] Hildebrand, R.H., Spillar, E.J., Stiening, R.F.: 1981, ApJ 243, 223-227.

[39] Hill, C.A., Smith, R.C., Hebb, L., Szkody, P.: 2017, MNRAS 472, 2937-2944.

[40] Holm A., Rice G.: 1981, NASA IUE Newslett., 15, 74

[41] Horne, K., Gomer, R.: 1980, ApJ 237, 845-849.

[42] Horne, J.H., Baliunas, S.L.: 1986, ApJ 302, 757-763.

[43] Howell, S.B., Cash, J., Mason, K.O., Herzog, A.E.: 1999, AJ 117, Issue 2, 1014-1022.

[44] Huang, S.-S.: 1972, ApJ 171, 549-564.

[45] Illarionov, A.F., Sunyaev, R.A.: 1975, A&A 39, 185.

[46] Joy, A.H.: 1956, ApJ 124, 317-320.

[47] Kiplinger, A.L.: 1979a, ApJ 234, 997-1015.

[48] Kiplinger, A.L.: 1979b, AJ 84, 655-660.

[49] Kjurkchieva, D., Marchev, D., Ogloza, W.: 1998, Ap&SS 262, Issue 1, 53-74.

[50] Körding, E., Rupen, M., Knigge, C., Fender, R., Dhawan, V., Templeton, M., Muxlow, T.: 2008, Sci 320, Issue 5881, 1318-1320.

[51] Lasota, J.P.: 2001, NewAR 45, Issue 7, 449-508.

[52] Lipunov, V.M.: 1987, Ap&SS 132, no. 1, 1-51.

[53] Lipunov, V.M., Postnov, K.A.: 1988, Ap&SS 145, no. 1, 1-45.

[54] Lipunov, V., Grinshpun, V., Vlasenko, D.: 2021, New Astron. Rev. 93, id. 101631.

[55] Lombardi, R., Giovannelli, F., Gaudenzi, S.: 1987, Ap&SS 130, Issue 1-2, 275-278.

[56] Marchev, D., Kjurkchieva, D., Ogloza, W.: 1999, AcA 49, 585-598.

[57] Martinez-Pais, I.G., Giovannelli, F., Rossi, C.; Gaudenzi, S.: 1994, A&A 291, 455-467.

[58] Mattei, J.A.: 1980, J. Roy. Astron. Soc. of Canada, Vol. 74, 317-320.

[59] Miller-Jones, J.C.A., Sivakoff, G.R., Knigge, C., Körding, E.G., Templeton, M., Waagen, E.O.: 2013, Science 340, Issue 6135, 950-952.

[60] Norton, A.J., Wynn, G.A., Somerscales, R.V.: 2004, ApJ 614, Issue 1, 349-357.

[61] Orosz, J.A., Remillard, R.A., Bailyn, C.D., McClintock, J.E.: 1997, ApJL 478, L83-L86.

[62] Pala, A.F., Gänsicke, B.T., Breedt, E., Knigge, C., Hermes, J.J. et al.: 2020, MNRAS 494, Issue 3, 3799-3827.

[63] Parkhurst, J.A., Zaccheus, D.: 1900, ApJ 12, 259-273.

[64] Patterson, J.: 1979, Ph.D. Thesis, The University of Texas at Austin (USA).

[65] Patterson, J.: 1981, APJ Suppl Ser. 45, 517-539.

[66] Patterson, J., Robinson, E.L., Kiplinger, A.L.: 1978, ApJ 226, L137-L139.

[67] Plavec, M.: 1968, in *Advances in Astronomy and Astrophysics, Volume 6*, Zdenêk Kopal (Ed.) pp. 201-278.

[68] Ponman T.J., Belloni T., Duck S.R., Verbunt F., Watson M.G., Wheatley P.J., Pfeffermann E.: 1995, MNRAS, 276, Issue 2, 495-504.

[69] Pringle J.E., Wade R.A. (eds.): 1985, *Interacting Binary Stars*, Cambridge Univ. Press

[70] Raguzova, N.V., Lipunov, V.M.: 1999, A&A 349, 505.

[71] Reimer, T.W., Welsh, W.F., Mukai, K., Ringwald, F.A.: 2008, ApJ 678, Issue 1, 376-384.

[72] Ricketts, M.J., King, A.R., Raine, D.J.: 1979, MNRAS 186, 233-244.

[73] Roberts, D.H., Lehar, J., Dreher, J.W.: 1987, A.J., 93, 968-989.

[74] Scargle, J.D.: 1982, ApJ 263, 835-853.

[75] Scaringi, S., Bird, A.J., Norton, A.J., Knigge, C., Hill, A.B. et al.: 2010, MNRAS 401, Issue 4, 2207-2218.

[76] Schreiber, M.R., Gänsicke, B.T.: 2002, A&A 382, 124-129.

[77] Schreiber, M.R., Lasota, J.-P.: 2007, A&A 473, Issue 3, 897-901.

[78] Shahbaz, T., Bandyopadhyay, R.M., Charles, P.A., Wagner, R.M., Muhli, P., et al.: 1998, MNRAS 300, 1035-1040.

[79] Shannon, C.: 1949, Proc. IEEE 37, 10-21.

[80] Smak, J.: 1967, AcA, 17, 255-270.

[81] Smak, J.: 1969, AcA 119, 155-164.

[82] Smak, J.: 1981, AcA 31, 395-408.

[83] Smak, J.: 1984, PASP 96, 5-18.

[84] Smak, J.: 1985a, in *Multifrequency Behaviour of Galactic Accreting Sources*, F. Giovannelli (ed.), SIDEREA, Roma, Italy, pp. 3-16.

[85] Smak, J.: 1985b, in *Multifrequency Behaviour of Galactic Accreting Sources*, F. Giovannelli (ed.), SIDEREA, Roma, Italy, pp. 17-36.

[86] Smak, J.: 1998, AcA 48, 677-693.

[87] Stover, R.J., Robinson, E.L., Nather, R.E., Montemayor, T.J.: 1980, ApJ 240, 597-607.

[88] Szkody, P., Michalsky, J.J., Stokes, G.M.: 1982, PASP 94, 137-142.

[89] Tramontana, V.: 2007, Thesis in Physics, University La Sapienza, Roma.

[90] Warner, B.: 1987, MNRAS 227, 23-73.

[91] Warner, B.: 1996, Ap&SS 241, Issue 2, 263-294.

[92] Warner, B., Wickramasinghe, D.T.: 1991, MNRAS 248, 370-376.

[93] Watson, M.G., King, A.R., Heise, J.: 1985, SSRv 40, Issue 1-2, 127-133.

[94] Wheatley, P.J., Mauche, C.W., Mattei, J.A.: 2003, MNRAS 345, Issue 1, 49-61.

[95] Zuckerman, M.-C. 1961, Annales d'Astrophysique 24, 431.